Structural basis of FANCD2 deubiquitination by USP1-UAF1

Martin L. Rennie[1]*, Connor Arkinson[1,2], Viduth K. Chaugule[1,2], Rachel Toth[2], Helen Walden[1,2]*

[1]Institute of Molecular Cell and Systems Biology, College of Medical Veterinary and Life Sciences, University of Glasgow, Glasgow, UK

[2]MRC Protein Phosphorylation and Ubiquitylation Unit, College of Life Sciences, University of Dundee, Dundee, UK

*Corresponding authors: Walden, Helen (Helen.Walden@glasgow.ac.uk); Rennie, Martin (Martin.Rennie@glasgow.ac.uk)

Keywords: ubiquitin, specificity, DNA repair, Fanconi Anemia, cryo-EM

Abstract

Ubiquitin-Specific Protease 1 (USP1) acts together with the cofactor UAF1 during DNA repair processes to specifically remove mono-ubiquitin signals. One substrate of the USP1-UAF1 complex is the mono-ubiquitinated FANCI-FANCD2 heterodimer, which is involved in the repair of DNA interstrand crosslinks via the Fanconi Anemia pathway. Here we determine structures of human USP1-UAF1 with and without ubiquitin, and bound to mono-ubiquitinated FANCI-FANCD2. The crystal structures of USP1-UAF1 reveal plasticity in USP1 and key differences to USP12-UAF1 and USP46-UAF1, two related proteases. A cryoEM reconstruction of USP1-UAF1 in complex with mono-ubiquitinated FANCI-FANCD2 highlights a highly orchestrated deubiquitination process with USP1-UAF1 driving conformational changes in the substrate. An extensive interface between UAF1 and FANCI, confirmed by mutagenesis and biochemical assays, provides a molecular explanation for the requirement of both proteins despite neither being directly involved in catalysis. Overall, our data provide molecular details of USP1-UAF1 regulation and substrate recognition.

Introduction

Ubiquitination is a reversible post-translation modification involving the attachment of ubiquitin, which acts as a signal to regulate numerous cellular pathways, including protein degradation, DNA replication, and DNA repair[1,2]. The attachment of ubiquitin proceeds via a cascade of enzymes and typically involves formation of an isopeptide bond between a lysine on the substrate and the carboxy-terminus of ubiquitin. Removal of the ubiquitin signal is achieved by a group of proteases known as deubiquitinases.

Ubiquitin signals are structurally diverse[1,2], composed of either poly-ubiquitin linkages, where different ubiquitin lysines are sequentially modified, or mono-ubiquitination, in which a single ubiquitin is attached to the target protein. Ubiquitin(s) can be directly recognised by reader proteins and/or result in direct conformational changes of the modified target protein for downstream effects. Signal reversal by deubiquitinases involves recognition of poly-ubiquitin or mono-ubiquitin substrates and hydrolysis of the isopeptide bond in a highly regulated manner[2,3].

The largest family of deubiquitinases are the Ubiquitin-Specific Proteases (USPs). DNA repair mechanisms including the Fanconi Anemia pathway utilize a member of this family, ubiquitin carboxyl-terminal hydrolase 1 (USP1), for deubiquitination of mono-ubiquitinated targets[4–8]. Loss of USP1 leads to dysfunctional DNA repair and genomic instability[5,7,8], and USP1 has been identified as a potential drug target for overcoming cancer resistance to DNA damaging drug treatment[9–11]. While we now understand how certain deubiquitinases specifically target

ubiquitin-ubiquitin linkages, how USP1 targets a specific set of ubiquitin-substrate linkages remains an open question.

Three key substrates of USP1 are PCNA, FANCI, and FANCD2, each of which is mono-ubiquitinated at a specific lysine residue during repair of DNA damage[5,6,12,13]. FANCI and FANCD2 can form a heterodimer, while PCNA forms a homotrimer, with both complexes able to form DNA clamps[14–16]. FANCI and FANCD2 are homologous proteins, each with an α-solenoid fold contorted into a saxophone shape[17]. The non-ubiquitinated FANCI-FANCD2 complex is stabilized by extensive interactions across the N-Terminal Domains (NTDs; residues 1-549 and 45-586, respectively) of each protein that partially bury the ubiquitination sites. The C-Terminal Domains (CTDs; residues 805-1280 and 929-1376, respectively) extend away from this interface to make an open trough, with the Helical Domain (HD; residues 550-804 and 587-928, respectively) connecting the NTD and CTD[15]. Recently, cryogenic electron microscopy (cryo-EM) reconstructions of mono-ubiquitinated FANCI-FANCD2 revealed a closed conformation of the heterodimer, resulting in it encircling DNA[15,16,18]. The ubiquitin conjugated to each subunit makes non-covalent contacts with the NTD of the other subunit, reconfiguring the NTD-NTD interface and creating a CTD-CTD interface. Mono-ubiquitination of the FANCD2 subunit alone is sufficient to induce this closed conformation and results in an enhanced affinity for double stranded DNA[15,16,18,19]. The ubiquitin signal has therefore been proposed to protect DNA during repair or may recruit other repair factors. How this specific ubiquitin signal is removed to unclamp FANCI-FANCD2 post-repair is not well understood.

USP1 contains a predicted Ubiquitin-Specific Protease (USP) catalytic fold with two large insertions and an N-Terminal Extension (NTE)[20]. USP1-Associated Factor (UAF1), which

enhances catalytic activity of USP1, USP12 and USP46[21,22], is composed of a β-propeller domain, an ancillary domain, and a SUMO-like domain (SLD). The β-propeller directly interacts with both USP12[23,24] and USP46[25,26] in the same way, a feature likely conserved for USP1[23]. The SLD is thought to mediate substrate recognition via binding to SUMO-Like domain Interacting Motifs (SLIMs) on substrates[23,25,27]. However, unlike USP1-UAF1, neither USP12-UAF1 nor USP46-UAF1 target mono-ubiquitinated FANCI-FANCD2[22]. Furthermore, FANCI buries a substantial surface of FANCD2's ubiquitin[15,16], which shields it from several deubiquitinases but not USP1-UAF1 *in vitro*[18]. Instead, FANCI phosphorylation is reported to impede USP1-UAF1 activity[28,29]; the underlying mechanism of this regulation remains unclear. Recently, biochemical work has shown that the NTE of USP1 is critical for specific removal of FANCD2's ubiquitin[20]. However a detailed understanding of how this specialized deubiquitinase targets ubiquitin sequestered within the FANCI-FANCD2 complex is hampered by the lack of structural information.

Here we present structures of human USP1-UAF1 alone, bound to ubiquitin, and finally bound to a mono-ubiquitinated FANCI-FANCD2 substrate, representing the first human deubiquitinase in complex with mono-ubiquitinated substrate. These structures provide insight into the catalytic cycle of USP1-UAF1. Crystal structures of truncated USP1-UAF1, with and without ubiquitin, reveal features shared with USP12/46-UAF1 complexes, and those that aid USP1's enzymatic activity. A cryo-EM structure of full-length USP1-UAF1 bound to FANCI and mono-ubiquitinated FANCD2 reveals an extensive UAF1-FANCI interface that surprisingly does not involve the previously predicted FANCI SLIM. Conformational changes are observed in each entity of the deubiquitinase-substrate complex, in particular FANCD2's ubiquitin disengages from FANCI and associates with USP1. In addition, the structures reveal how engagement of

96 USP1-UAF1 can occur while the FANCI-FANCD2 heterodimer is clamped on DNA. Using
97 mutational analyses and biochemical assays we highlight the importance of the interfaces
98 within the structures. Overall the structures and assays clarify a highly orchestrated and
99 multifaceted deubiquitination cycle, in which two binding partner proteins, UAF1 and FANCI,
100 along with USP1 contacts with FANCD2, regulate the reversal of this critical ubiquitin signal.

101

102 **Results**

103 *Architecture and plasticity of USP1*

104 In order to understand how USP1 is regulated by UAF1 and how USP1 targets ubiquitin, we
105 sought to determine structures of multiple stages in USP1's catalytic cycle. We determined
106 structures of USP1-UAF1 with and without ubiquitin using X-ray crystallography. Full-length
107 constructs of USP1-UAF1 did not yield well-diffracting crystals. In order to obtain USP1-UAF1
108 crystals that diffract to better than 4 Å, we deleted several flexible regions of USP1, predicted
109 to be disordered, and the SLD of UAF1 (Fig. 1a, Methods, Table 1). We determined a ubiquitin-
110 bound structure of the same construct by reacting USP1 with propargylated ubiquitin[30] (Fig.
111 1b). The USP1 structure exhibits a typical "fingers-palm-thumb" architecture (Fig. 1a). Ubiquitin
112 sits in the hand, making contacts with all three subdomains, while only the fingers interact with
113 UAF1's β-propeller domain, as observed for USP12-UAF1[23,24] and USP46-UAF1[25]. Approximately
114 40% of the ubiquitin surface, including the hydrophobic patch, is covered by the USP1 hand,
115 similar to other deubiquitinases[31]. Like the other USP-UAF1 complexes, the interaction surface
116 between the USP1 fingers and UAF1 β-propeller is relatively small, burying a surface area of

~800 Å, and contains numerous charged and polar residues (Fig. 1c). The deleted Inserts 1 and 2 are positioned on the opposite face of USP1 to the ubiquitin binding site, while the deleted N-terminus extends from the distal tip of USP1, furthest from UAF1 (Fig. 1b). In both crystal structures a 1:1 stoichiometry of USP1 to UAF1 was observed, whereas a previous study has suggested a 1:2 stoichiometry in solution[24]. To determine the stoichiometry of our crystallised construct in solution we used small angle X-ray scattering (SAXS) measurements. These measurements confirm the oligomeric arrangement and 1:1 stoichiometry observed in the crystal structures (Fig 1c, Extended Data Fig. 1a-c).

Comparison of the ubiquitin bound and unbound structures of USP1-UAF1 reveals conformational changes in USP1. In the ubiquitin-bound structure, "Binding Loops" BL1 and BL2 are re-arranged with respect to the ubiquitin-free structure, which allows threading of the ubiquitin tail between the palm and thumb (Fig. 1d), while the globular body of ubiquitin primarily contacts the fingers. In addition to these local changes, USP1 exhibits flexibility in the fingers, with a 30° rotation relating the palm and thumb of the two crystal structures (Fig. 1a-b). Furthermore, each crystal had two USP1-UAF1 complexes per asymmetric unit both with similar conformations within the same asymmetric unit (Extended Data Fig. 1d). Such structural plasticity has been also observed for crystal structures of USP12-UAF1[23,24] and USP46-UAF1[25] and may facilitate substrate engagement.

Although USP1, USP12, and USP46 are all regulated by UAF1, only USP12 and USP46 activities are enhanced by another cofactor, WDR20[32,33]. Several structural features of the ubiquitin-free USP1-UAF1 structure correspond more closely to WDR20-bound USP12 and USP46 structures than WDR20-free USP12[23,26] (Extended Data Fig. 1e-g). A conserved phenylalanine is buried

between the fingers and palm for USP1-UAF1 and USP12/46-UAF1-WDR20, but not USP12-UAF1 (Extended Data Fig. 1e). Correlating with this, there is a conformational change in the fingers with respect to the palm and thumb. In addition, USP1's BL1 is ordered in USP1-UAF1 and USP12/46-UAF1-WDR20 but not USP12-UAF1 (Extended Data Fig. 1f), however crystal packing effects of the ubiquitin-free USP1-UAF1 structure may contribute to this stabilization. These differences hint at the possibility the USP fold of USP1 may be primed for efficient catalysis without the additional requirement of WDR20. Overall, our crystal structures reveal typical USP-ubiquitin and USP-UAF1 interactions and highlight the differences between USP1 and USP12/46 along with the positioning of the inserts and NTE of USP1.

Structure of USP1-UAF1 bound to FANCI-FANCD2 substrate

Our USP1-UAF1 structures allow comparisons to USP12/46 complexes, demonstrate plasticity in the USP fold and show how USP1 binds ubiquitin. In order to understand how USP1-UAF1 recognises mono-ubiquitinated substrate, we determined a cryo-EM structure of full length USP1-UAF1 bound to the FANCI-FANCD2^{Ub}-DNA substrate with ubiquitin only on FANCD2. This singly mono-ubiquitinated substrate is readily deubiquitinated by USP1-UAF1 unlike the doubly mono-ubiquitinated complex, FANCI^{Ub}-FANCD2^{Ub} [18,20,34]. We employed a catalytically compromised C90S mutant of USP1, and our previous strategy for generating the mono-ubiquitinated substrate[35,36] to reconstitute the USP1^{C90S}-UAF1-FANCI-FANCD2^{Ub} complex, with full length versions of all four proteins (Extended Data Fig. 2a). We then determined a cryo-EM reconstruction of this enzyme-substrate complex, bound to double-stranded DNA, at 3.7 Å global resolution (FSC=0.143) and local resolution 3.4-9.9 Å (FSC=0.5) (Fig. 2a, Table 2, Extended Data Fig. 2b-g, Extended Data Fig. 3). Using our crystal structure of ubiquitin-bound USP1-UAF1

described above (Fig. 1), and the structures of mono-ubiquitinated human FANCI-FANCD2^{Ub} (PDB 6VAF[15]) and full-length UAF1 (PDB 5K1A[23]) we built a model of approximately 70% of the residues in the complex including the K561-G76 isopeptide linkage (Fig. 2b-c, Extended Data Fig. 2h). The N- and C-termini of FANCI and FANCD2, the USP1 inserts and NTE, several loops, and the DNA bases were left unmodelled due to low local resolution.

Globally, USP1-UAF1 and the ubiquitin of FANCD2 are in a similar arrangement to the ubiquitin-bound crystal structure described above (Fig. 1). FANCI-FANCD2 are in a closed conformation encircling DNA, similar to that observed for the singly and doubly monoubiquitinated complexes[15,16,18]. The enzyme-substrate complex is arranged such that USP1 contacts FANCD2 while UAF1 contacts FANCI in a 1:1:1:1 stoichiometry.

UAF1 and FANCI form a scaffold for deubiquitination

UAF1 and FANCI have an extensive interface that involves interactions from the β-propeller, ancillary, and SLD of UAF1 and the FANCI NTD and HD, and buries ~1600 Å^2 (Fig. 3a). Interestingly, a FANCI SLIM[27], previously proposed to mediate interactions with UAF1, was not located at the interface observed here. Instead, a FANCI loop (^{251}DELLDVV^{257}) directly interacts with the SLD of UAF1 (Fig. 3a), with L254 inserting into the SLD hydrophobic groove. This loop contains both hydrophobic and acidic residues and interacts with the SLD in a manner reminiscent of SUMO-like interacting motifs (SIMs; Extended Data Fig. 4)[37]. The UAF1-FANCI interface observed here likely explains how FANCI favours USP1-UAF1 targeting over more promiscuous deubiquitinases[18].

To further test this hypothesis, we compared the deubiquitination activity of USP1 reconstituted with either full-length UAF1, or UAF1 truncations lacking the SLD (UAF1$^{\Delta SLD}$), or comprising just the β-propeller domain (UAF1$^{\beta\text{-propeller}}$). Both truncations severely impair deubiquitination of FANCI-FANCD2^{Ub} compared to full-length UAF1 (Fig. 3b). To confirm that this was not due generic reduction in activity we also assessed deubiquitination of FANCD2^{Ub} in the absence of FANCI (Extended Data Fig. 5a-d). For the UAF1 truncations deubiquitination of FANCD2^{Ub} alone is only slightly reduced compared to full-length, as also reported for USP46-UAF1$^{\beta\text{-propeller}}$ acting on fluorescently tagged ubiquitin[25]. Indeed, even at enzyme concentrations resulting in comparable deubiquitination of FANCD2^{Ub} alone, activity against FANCI-FANCD2^{Ub} for the UAF1$^{\beta\text{-propeller}}$ is reduced compared to full-length UAF1, confirming the importance of the UAF1-FANCI interaction (Extended Data Fig. 5d). UAF1 increases the generic enzymatic activity of USP1[21]. Consistent with this, in the absence of UAF1 (USP1 alone) we did not detect deubiquitination of either substrate (Extended Data Fig. 5a-b). Overall, these data suggest that the SLD and Ancillary domain are important for deubiquitination in the context of the FANCI-FANCD2 heterodimer.

In addition, the β-propeller domain of UAF1 interacts with a loop connecting the NTD and HD of FANCI (FANCI$^{547\text{-}576}$), the phosphorylation of which inhibits deubiquitination by USP1-UAF1[28,29] (Fig. 3a). Although density for the FANCI phosphorylation targets (S556, S559, and S565) is weak in our reconstruction, neighbouring residues contribute hydrophobic interactions and backbone hydrogen bonds to the interaction. We confirmed a role of FANCI phosphorylation in regulating FANCI-FANCD2^{Ub} deubiquitination using different FANCI mutants (Fig. 3c, Extended Data Fig. 5e). The addition of FANCI phosphomimic S556D-S559D or S556D-S559D-S565D mutants result

in reduced FANCD2 deubiquitination compared to addition of wild-type FANCI. On the other hand, phosphodead S556A-S559A or S556A-S559A-S565A mutants are similar to wild-type. Finally, we note that mutation of the previously proposed SLIM motif of FANCI[27] (I683A-L685A) results in similar deubiquitination to wild-type FANCI, confirming its redundancy for FANCI-FANCD2^{Ub} deubiquitination *in vitro* (Extended Data Fig. 5e). We propose that the altered electrostatics of FANCI$^{547-576}$, due to phosphorylation, reduces competency for binding to UAF1. Supporting this hypothesis, we detect reduced binding of the phosphomimic S556D-S559D-S565D compared to the phosphodead S556A-S559A-S565A mutant, by Microscale Thermophoresis (MST; Extended Data Fig. 5f-g). Taken together, the extensive UAF1-FANCI interface, along with FANCI phosphorylation influence efficient USP1-UAF1 activity and reveal the multi-faceted regulation underlying FANCD2 deubiquitination.

Ubiquitin is poised for removal from FANCD2

The ubiquitin conjugated to FANCD2 undergoes a large rearrangement in the enzyme-substrate, USP1-UAF1-FANCI-FANCD2^{Ub}, complex relative to the substrate only, FANCI-FANCD2^{Ub}, complex (Fig. 4a, Supplementary Video 1). In the FANCI-FANCD2^{Ub} complex, the ubiquitin tail is bent in a conformation incompatible with USP1 binding, with ubiquitin R72 forming intramolecular interactions with FANCD2 and the ubiquitin hydrophobic patch forming intermolecular interactions with FANCI[15,16]. In the USP1-UAF1-FANCI-FANCD2^{Ub} complex, ubiquitin is rotated by 160° and extracted from its non-covalent interaction with FANCI to sit in the hand of USP1, with the ubiquitin tail extended to sit between the palm and thumb (Fig. 4a, Extended Data Fig. 6a). The resulting USP1-ubiquitin interaction is analogous to the ubiquitin-

bound crystal structure above (Fig. 1b), however the palm and thumb are slightly more contracted with respect to the fingers (Extended Data Fig. 6b).

While the USP1-ubiquitin interaction buries ~1800 Å^2, the observed USP1-FANCD2 interaction is significantly smaller, burying ~600 Å^2. Within the USP1-FANCD2 interface, a conserved arginine on FANCD2 (R560), adjacent to the ubiquitinated lysine, hydrogen bonds with D751 of USP1 (Fig. 2c). This aspartate also hydrogen bonds with H593 and together with C90 forms the catalytic triad. The coordination of R560 may indirectly assist catalysis by adding to the stability of H593 in a conformation ready to deprotonate C90.

Sitting at the crux between FANCI, FANCD2, and the BL1 of USP1 is weak density (Extended Data Fig. 6c, 7). Given its location it likely belongs to the tip of BL1, however we were not able to unambiguously build or assign this density. Contributing to this uncertainty, the NTE density terminates adjacent to the USP domain and FANCD2 (Extended Data Fig. 6d), leaving 74 residues unmodelled. Density for Inserts 1 and 2 of USP1 is absent in our structure (Extended Data Fig. 6e), suggesting that these are not tightly associated with the USP domain and consistent with their disposability for FANCI and FANCD2 deubiquitination[20]. An isoleucine on the BL2 loop of USP1 inserts into a hydrophobic pocket of FANCD2, while in USP12/46 this position is occupied by a polar residue (Extended Data Fig. 7). Overall it seems that BL1 and BL2 in USP1 are specialized for deubiquitination of FANCD2 compared to USP12/46.

The closed conformation of FANCI-FANCD2 is recognised by USP1-UAF1

The FANCI-FANCD2 heterodimer remains in the closed conformation that encircles DNA when USP1-UAF1 is bound, despite disruption of the non-covalent interaction between FANCD2's ubiquitin and FANCI (Fig. 2a). The open, trough shaped FANCI-FANCD2 conformation would be

incompatible with the mode of USP1-UAF1 binding identified here due to steric clashes with USP1 (Fig. 4a, bottom panel). However, the FANCD2 subunit adopts an intermediate conformation to the ubiquitinated and non-ubiquitinated extremes (Fig. 4b). The NTD of FANCD2 was previously shown to flex with respect to the CTD, adopting an extended conformation in unmodified FANCD2 and bent when it is ubiquitinated[15]. When bound to USP1-UAF1, the NTD of FANCD2 becomes more extended than the ubiquitinated extreme, however retains some flexibility as illustrated by 3D variability analysis[38] (Supplementary Videos 2-4).

Although residues 1-180 of FANCI had weak density and were not modelled for our structure, the rest of FANCI remains in a globally similar conformation regardless of ubiquitination state or binding of USP1-UAF1 (Fig. 4c). However, there are slight changes in the region 437-790, encompassing part of the NTD and most of the HD, including the FANCI ubiquitination site. The USP1-UAF1 bound state more closely aligns with the non-ubiquitinated state, particularly for helices 511-526, 530-546, and 577-594 (Fig. 4c). These helices are adjacent UAF1 β-propeller binding site and contain the FANCI mono-ubiquitination site (K523). Interestingly, the other face of this region contacts the FANCD2 NTD and the ubiquitin of FANCI in the doubly mono-ubiquitinated state[15]. There is sufficient space within the USP1-UAF1 bound complex to accommodate the ubiquitin of FANCI (Extended Data Fig. 6f). As such steric occlusion cannot account for the reduced deubiquitination when FANCI is also ubiquitinated. Instead we propose that FANCI interaction with UAF1 regulates the interaction between FANCI and FANCD2 and that mono-ubiquitination of FANCI also regulates these interactions.

Discussion

The structures described here provide insight into the catalytic cycle of USP1-UAF1 deubiquitination and mechanisms by which the cycle is controlled (Fig. 5). The ubiquitin-free crystal structure (Fig. 1a) represents the free enzyme (E), while the cryo-EM structure (Fig. 2b) represents a substrate-bound state (ES), in which the enzyme has globally distorted the substrate. Local changes in the active site are further required to distort the isopeptide bond into the transition state before hydrolysis occurs. Subsequent dissociation of deubiquitinated FANCI-FANCD2 in the open conformation (P) likely occurs prior to dissociation of ubiquitin, as occurs for other USPs[39]. We reason that this would occur due to the narrow size of the pocket through which ubiquitin could leave the in the USP1-UAF1-FANCI-FANCD2^{Ub} structure, and the conformational changes occurring that appear to be restoring the open conformations of the FANCI and FANCD2 subunits. Finally, ubiquitin-bound enzyme (EP), represented here by the ubiquitin-bound crystal structure (Fig. 1b), must release ubiquitin to complete the catalytic cycle.

Enzymes acting on large proteins typically utilize various regions of the substrate and the enzyme distal to the active site, to facilitate catalysis[40]. The USP1-UAF1 enzyme and FANCI-FANCD2^{Ub} substrate are prime examples of this complexity, with regulation occurring at multiple places (Fig. 5). Furthermore, in this system, two relatively rigid subunits, UAF1 of the enzyme complex and FANCI of the substrate complex, appear to act as a scaffold, while the catalytic subunit, USP1, and the ubiquitin and conjugated protein, FANCD2, are much more flexible. Such flexibility may be an essential feature of the machinery, allowing for gross conformational changes to occur, much in the same way local rearrangements of a catalytic site are required in enzymes acting on small molecules.

Although we were unable to unambiguously locate the NTE of USP1, which we have previously shown is necessary for efficient deubiquitination of FANCD2[20], we did identify a candidate region for the extended BL1 of USP1 (Extended Data Fig. 6c, 7). Curiously, the region identified sits between FANCI and FANCD2 with two aromatic residues in close proximity (FANCI^{F277} and FANCD2^{Y520}). Both of these residues are buried by the NTD-NTD interface in the open, non-ubiquitinated FANCI-FANCD2 state. As such the occupant of the density may maintain the closed conformation while FANCI and FANCD2 return to their respective open conformations.

In terms of the FA pathway, our structures demonstrate that USP1 can recognize the FANCI-FANCD2 complex clamped on DNA. Given the UAF1-FANCI interaction and the importance of UAF1 for USP1 isopeptidase activity[21], it seems that the USP1-UAF1 deubiquitinase complex is organised to recognise the FANCI-FANCD2 heterodimer. Upon completion of the deubiquitination reaction and dissociation of USP1-UAF1, FANCI-FANCD2 likely returns to the open conformation, unclamping it from DNA. Therefore the likely role of USP1-UAF1 in the FA pathway is to release FANCI-FANCD2 from DNA, post-repair, to allow the replication machinery to continue.

The role of DNA in the regulation of deubiquitination is unclear, with studies reporting DNA-mediated inhibition[18,20,34] and enhancement[41,42] of deubiquitination, however mono-ubiquitination of FANCI plays a critical role. Such discrepancies may originate from DNA binding to FANCI-FANCD2 or USP1-UAF1, respectively, or from differences in the extent of mono-ubiquitinated FANCI during sample preparation. Despite addition of dsDNA after formation of the enzyme-substrate complex we did not find evidence of DNA binding to USP1-UAF1 suggesting dsDNA preferentially binds to FANCI-FANCD2^{Ub}. ithin the USP1-UAF1-FANCI-

FANCD2^{Ub} structure there is space to accommodate ubiquitin conjugated to FANCI (Extended Data Fig. 6f). As such we expect a similar mechanism for recognition of FANCI^{Ub}-FANCD2^{Ub} for FANCD2 deubiquitination, as FANCI-FANCD2^{Ub}. FANCD2 is deubiquitinated more slowly in the FANCI^{Ub}-FANCD2^{Ub} complex with I44 of FANCI's ubiquitin playing an important role[18,20,34]. The interaction between FANCI's ubiquitin and FANCD2's NTD[15] may restrict flexing of the NTD observed in the USP1-UAF1-FANCI-FANCD2^{Ub} structure (Fig. 4b). Alternatively, the conjugation of ubiquitin to FANCI may reduce the propensity for USP1-UAF1 to return the FANCI subunit to its open conformational state. Indeed the mono-ubiquitinated lysine of FANCI (K523) lies on one of the helices that is perturbed by USP1-UAF1 binding (Fig. 3c). Either or both of these would provide a mechanism for the protection of FANCD2 from deubiquitination that is achieved by FANCI ubiquitination. Although the order of deubiquitination of FANCI^{Ub}-FANCD2^{Ub} is not known, the FANCD2 subunit is more rapidly deubiquitinated in biochemical assays and therefore expected to be deubiquitinated first. How FANCI is deubiquitinated remains an open question and will require further enzyme-substrate structures.

Although USP1 and FANCI compete for the hydrophobic patch of ubiquitin, the surface area of ubiquitin buried by FANCI (1450 Å^2)[15] is less than that of USP1. As the FANCI binding surface is remains accessible in our structure, the larger surface buried by USP1 may allow for preferential binding of ubiquitin to USP1 over FANCI. In the doubly mono-ubiquitinated complex, the surface area of the ubiquitin conjugated to FANCI, buried by FANCD2 is 1820 Å^2 [15]. Therefore, it may be more difficult for USP1-UAF1 to extract the ubiquitin conjugated to FANCI from the complex, consistent with the observation that deubiquitination of FANCD2's ubiquitin occurs more rapidly than FANCI's ubiquitin[18,20,34].

Finally, we have revealed the mechanism of FANCI recognition by UAF1 (Fig. 3). Unlike the NTE of USP1, which facilitates deubiquitination of FANCD2 in general[20], the UAF1-FANCI interface facilitates deubiquitination in the context of the FANCI-FANCD2 heterodimer. This interface appears to act as a switchable substrate adaptor, allowing USP1 to target ubiquitinated FANCD2 when FANCI is dephosphorylated. In addition it contributes to the ability of USP1 to overcome the masking of the hydrophobic patch of ubiquitin by FANCI. The FANCI region containing the S556, S559, and S565 phosphorylation sites appears to be a key player in this interaction. Interestingly, crystal structures of mouse FANCI-FANCD2 (3S4W) and FANCI alone (3S51) show this region two different conformations[17], while in cryo-EM structures of human FANCI-FANCD2 without UAF1 the region is not well ordered (PDB 6VAA, PDB 6VAD, PDB 6VAE, PDB 6VAF)[15]. Therefore, the dynamics of this region may be important for regulating recognition by UAF1. UAF1 facilitates deubiquitination of FANCI-FANCD2^{Ub} by a dual role of enhancing catalytic activity through binding to USP1 via the β-propeller domain and adding avidity to the substrate interaction via the SLD, ancillary, and β-propeller domains. Overall, our results reveal a sophisticated deubiquitination process in which multiple regions of the substrate are recognized to coordinate both ubiquitin removal and substrate conformation.

Acknowledgements

We thank past and current members of the Walden laboratory for experimental suggestions, comments on the manuscript and their support. All constructs are available on request from the MRC Protein Phosphorylation and Ubiquitylation Unit reagents Web page (http://mrcppureagents.dundee.ac.uk) or from the corresponding author. We acknowledge Diamond Light Source for time on beamline I04 (proposal mx14980) and B21 (proposal mx19844) and thank Dr. Nikul Khunti for collecting SAXS data. We acknowledge the Scottish Centre for Macromolecular Imaging (SCMI) for access to cryo-EM instrumentation, funded by the MRC (MC_PC_17135) and SFC (H17007), and thank Dr. Mairi Clarke and Dr. James Streetley for screening and collection of cryo-EM data. This work was supported by the European Research Council (ERC-2015-CoG-681582) ICLUb consolidator grant to H.W. and the Medical Research Council (MC_UU_120164/12).

Author contributions

M.L.R., C.A., V.K.C. and H.W. conceived this work; C.A., M.L.R. and V.K.C. purified proteins; C.A. and R.T. generated various expression vectors and performed mutagenesis; C.A. performed crystallography; C.A. performed SAXS data processing; M.L.R. performed cryo-EM data processing; M.L.R. and C.A. performed model building and refinement; M.L.R. performed assays; M.L.R. and C.A. wrote the manuscript with contributions from all other authors; H.W. secured funding and supervised the project.

Competing interests

The authors declare no competing interests.

References

1. Yau, R. & Rape, M. The increasing complexity of the ubiquitin code. *Nat. Cell Biol.* **18**, 579–586 (2016).

2. Mevissen, T. E. T. & Komander, D. Mechanisms of deubiquitinase specificity and regulation. *Annu. Rev. Biochem.* **86**, 159–192 (2017).

3. Grabbe, C., Husnjak, K. & Dikic, I. The spatial and temporal organization of ubiquitin networks. *Nat. Rev. Mol. Cell Biol.* **12**, 295–307 (2011).

4. Nijman, S. M. B. *et al.* The deubiquitinating enzyme USP1 regulates the fanconi anemia pathway. *Mol. Cell* **17**, 331–339 (2005).

5. Huang, T. T. *et al.* Regulation of monoubiquitinated PCNA by DUB autocleavage. *Nat. Cell Biol.* **8**, 339–347 (2006).

6. Sims, A. E. *et al.* FANCI is a second monoubiquitinated member of the Fanconi anemia pathway. *Nat. Struct. Mol. Biol.* **14**, 564–567 (2007).

7. Oestergaard, V. H. *et al.* Deubiquitination of FANCD2 Is Required for DNA Crosslink Repair. *Mol. Cell* **28**, 798–809 (2007).

8. Murai, J. *et al.* The USP1/UAF1 Complex Promotes Double-Strand Break Repair through Homologous Recombination. *Mol. Cell. Biol.* **31**, 2462–2469 (2011).

9. Chen, J. *et al.* Selective and cell-active inhibitors of the USP1/ UAF1 deubiquitinase complex reverse cisplatin resistance in non-small cell lung cancer cells. *Chem. Biol.* **18**, 1390–1400 (2011).

10. García-Santisteban, I., Peters, G. J., Giovannetti, E. & Rodríguez, J. A. USP1 deubiquitinase: Cellular functions, regulatory mechanisms and emerging potential as target in cancer therapy. *Mol. Cancer* **12**, 1–12 (2013).

11. Liang, Q. *et al.* A selective USP1-UAF1 inhibitor links deubiquitination to DNA damage responses. *Nat. Chem. Biol.* **10**, 298–304 (2014).

12. Garcia-Higuera, I. *et al.* Interaction of the Fanconi anemia proteins and BRCA1 in a common pathway. *Mol. Cell* **7**, 249–262 (2001).

13. Smogorzewska, A. *et al.* Identification of the FANCI Protein, a Monoubiquitinated FANCD2

Paralog Required for DNA Repair. *Cell* **129**, 289–301 (2007).

14. Krishna, T. S. R., Kong, X. P., Gary, S., Burgers, P. M. & Kuriyan, J. Crystal structure of the eukaryotic DNA polymerase processivity factor PCNA. *Cell* **79**, 1233–1243 (1994).

15. Wang, R., Wang, S., Dhar, A., Peralta, C. & Pavletich, N. P. DNA clamp function of the monoubiquitinated Fanconi anaemia ID complex. *Nature* **580**, 278–282 (2020).

16. Alcón, P. *et al.* FANCD2–FANCI is a clamp stabilized on DNA by monoubiquitination of FANCD2 during DNA repair. *Nat. Struct. Mol. Biol.* **27**, 240–248 (2020).

17. Joo, W. *et al.* Structure of the FANCI-FANCD2 complex: Insights into the Fanconi anemia DNA repair pathway. *Science* **333**, 312–316 (2011).

18. Rennie, M. L. *et al.* Differential functions of FANCI and FANCD2 ubiquitination stabilize ID2 complex on DNA. *EMBO Rep.* e50133 (2020). doi:10.15252/embr.202050133

19. Tan, W. *et al.* Monoubiquitination by the human Fanconi Anemia core complex clamps FANCI:FANCD2 on DNA in filamentous arrays. *Elife* **9**, e54128 (2020).

20. Arkinson, C., Chaugule, V. K., Toth, R. & Walden, H. Specificity for deubiquitination of monoubiquitinated FANCD2 is driven by the N-terminus of USP1. *Life Sci. Alliance* **1**, e201800162 (2018).

21. Cohn, M. A. *et al.* A UAF1-Containing Multisubunit Protein Complex Regulates the Fanconi Anemia Pathway. *Mol. Cell* **28**, 786–797 (2007).

22. Cohn, M. A., Kee, Y., Haas, W., Gygi, S. P. & D'Andrea, A. D. UAF1 is a subunit of multiple deubiquitinating enzyme complexes. *J. Biol. Chem.* **284**, 5343–5351 (2009).

23. Li, H. *et al.* Allosteric Activation of Ubiquitin-Specific Proteases by β-Propeller Proteins UAF1 and WDR20. *Mol. Cell* **63**, 249–260 (2016).

24. Dharadhar, S., Clerici, M., van Dijk, W. J., Fish, A. & Sixma, T. K. A conserved two-step binding for the UAF1 regulator to the USP12 deubiquitinating enzyme. *J. Struct. Biol.* **196**, 437–447 (2016).

25. Yin, J. *et al.* Structural Insights into WD-Repeat 48 Activation of Ubiquitin-Specific Protease 46. *Structure* **23**, 2043–2054 (2015).

26. Zhu, H., Zhang, T., Wang, F., Yang, J. & Ding, J. Structural insights into the activation of USP46 by

WDR48 and WDR20. *Cell Discov.* **5**, 1–4 (2019).

27. Yang, K. *et al.* Regulation of the Fanconi anemia pathway by a SUMO-like delivery network. *Genes Dev.* **25**, 1847–1858 (2011).

28. Cheung, R. S. *et al.* Ubiquitination-Linked Phosphorylation of the FANCI S/TQ Cluster Contributes to Activation of the Fanconi Anemia I/D2 Complex. *Cell Rep.* **19**, 2432–2440 (2017).

29. Tan, W., van Twest, S., Murphy, V. J. & Deans, A. J. ATR-Mediated FANCI Phosphorylation Regulates Both Ubiquitination and Deubiquitination of FANCD2. *Front. Cell Dev. Biol.* **8**, 2 (2020).

30. Ekkebus, R. *et al.* On terminal alkynes that can react with active-site cysteine nucleophiles in proteases. *J. Am. Chem. Soc.* **135**, 2867–2870 (2013).

31. Komander, D., Clague, M. J. & Urbé, S. Breaking the chains: Structure and function of the deubiquitinases. *Nat. Rev. Mol. Cell Biol.* **10**, 550–563 (2009).

32. Kee, Y. *et al.* WDR20 regulates activity of the USP12·UAF1 deubiquitinating enzyme complex. *J. Biol. Chem.* **285**, 11252–11257 (2010).

33. Dahlberg, C. L. & Juo, P. The WD40-repeat Proteins WDR-20 and WDR-48 Bind and activate the Deubiquitinating Enzyme USP-46 to promote the abundance of the Glutamate Receptor GLR-1 in the ventral Nerve Cord of Caenorhabditis elegans. *J. Biol. Chem.* **289**, 3444–3456 (2014).

34. van Twest, S. *et al.* Mechanism of Ubiquitination and Deubiquitination in the Fanconi Anemia Pathway. *Mol. Cell* **65**, 247–259 (2017).

35. Chaugule, V. K., Arkinson, C., Toth, R. & Walden, H. Enzymatic preparation of monoubiquitinated FANCD2 and FANCI proteins. *Methods Enzymol.* **618**, 73–104 (2019).

36. Chaugule, V. K. *et al.* Allosteric mechanism for site-specific ubiquitination of FANCD2. *Nat. Chem. Biol.* **16**, 291–301 (2020).

37. Kerscher, O. SUMO junction—what's your function? New insights through SUMO-interacting motifs. *EMBO Rep.* **8**, 550–555 (2007).

38. Punjani, A. & Fleet, D. J. 3D variability analysis : Directly resolving continuous flexibility and discrete heterogeneity from single particle cryo-EM images. *bioRxiv* (2020). doi:10.1101/2020.04.08.032466.

39. Clerici, M., Luna-Vargas, M. P. A., Faesen, A. C. & Sixma, T. K. The DUSP-Ubl domain of USP4 enhances its catalytic efficiency by promoting ubiquitin exchange. *Nat. Commun.* **5**, (2014).

40. Rennie, M. L., Chaugule, V. K. & Walden, H. Modes of allosteric regulation of the ubiquitination machinery. *Curr. Opin. Struct. Biol.* **62**, 189–196 (2020).

41. Lim, K. S. *et al.* USP1 Is Required for Replication Fork Protection in BRCA1-Deficient Tumors. *Mol. Cell* **72**, 925-941.e4 (2018).

42. Liang, F. *et al.* DNA requirement in FANCD2 deubiquitination by USP1-UAF1-RAD51AP1 in the Fanconi anemia DNA damage response. *Nat. Commun.* **10**, 1–8 (2019).

43. Pace, N. C., Vajdos, F., Fee, L., Grimsley, G. & Gray, T. How to Measure and Predict the Molar Absorption Coefficient of a Protein. *Protein Sci.* **4**, 2411–2423 (1995).

44. Battye, T. G. G., Kontogiannis, L., Johnson, O., Powell, H. R. & Leslie, A. G. W. iMOSFLM: A new graphical interface for diffraction-image processing with MOSFLM. *Acta Cryst. D* **67**, 271–281 (2011).

45. Evans, P. R. & Murshudov, G. N. How good are my data and what is the resolution? *Acta Cryst. D* **69**, 1204–1214 (2013).

46. McCoy, A. J. *et al.* Phaser crystallographic software. *J. Appl. Crystallogr.* **40**, 658–674 (2007).

47. Emsley, P., Lohkamp, B., Scott, W. G. & Cowtan, K. Features and development of Coot. *Acta Cryst. D* **66**, 486–501 (2010).

48. Murshudov, G. N. *et al.* REFMAC5 for the refinement of macromolecular crystal structures. *Acta Cryst. D* **67**, 355–367 (2011).

49. Liebschner, D. *et al.* Macromolecular structure determination using X-rays, neutrons and electrons: Recent developments in Phenix. *Acta Crystallogr. Sect. D Struct. Biol.* **75**, 861–877 (2019).

50. Franke, D. *et al.* ATSAS 2.8: A comprehensive data analysis suite for small-angle scattering from macromolecular solutions. *J. Appl. Crystallogr.* **50**, 1212–1225 (2017).

51. Hopkins, J. B., Gillilan, R. E. & Skou, S. BioXTAS RAW: Improvements to a free open-source program for small-angle X-ray scattering data reduction and analysis. *J. Appl. Crystallogr.* **50**,

1545–1553 (2017).

52. Mastronarde, D. N. Automated electron microscope tomography using robust prediction of specimen movements. *J. Struct. Biol.* **152**, 36–51 (2005).

53. Zivanov, J. *et al.* New tools for automated high-resolution cryo-EM structure determination in RELION-3. *Elife* **7**, e42166 (2018).

54. Punjani, A., Rubinstein, J. L., Fleet, D. J. & Brubaker, M. A. CryoSPARC: Algorithms for rapid unsupervised cryo-EM structure determination. *Nat. Methods* **14**, 290–296 (2017).

55. Punjani, A., Zhang, H. & Fleet, D. J. Non-uniform refinement: adaptive regularization improves single-particle cryo-EM reconstruction. *Nat. Methods* **17**, 1214–1221 (2020).

56. Sanchez Garcia, R. *et al.* DeepEMhacer: a deep learning solution for cryo-EM volume post-processing. *bioRxiv* (2020). doi:10.1101/2020.06.12.148296

57. Cianfrocco, M. A., Wong-Barnum, M., Youn, C., Wagner, R. & Leschziner, A. COSMIC2: A science gateway for cryo-electron microscopy structure determination. in *Practice & Experience in Advanced Research Computing* New Orleans, LA Jul 9-13 (2017). doi:10.1145/3093338.3093390

58. Pettersen, E. F. *et al.* UCSF Chimera - A visualization system for exploratory research and analysis. *J. Comput. Chem.* **25**, 1605–1612 (2004).

59. Afonine, P. V. *et al.* Real-space refinement in PHENIX for cryo-EM and crystallography. *Acta Crystallogr. Sect. D Struct. Biol.* **74**, 531–544 (2018).

60. Krissinel, E. & Henrick, K. Inference of Macromolecular Assemblies from Crystalline State. *J. Mol. Biol.* **372**, 774–797 (2007).

61. Goddard, T. D. *et al.* UCSF ChimeraX: Meeting modern challenges in visualization and analysis. *Protein Sci.* **27**, 14–25 (2018).

62. Hunter, J. D. Matplotlib: A 2D graphics environment. *Comput. Sci. Eng.* **9**, 90–95 (2007).

63. Baba, D. *et al.* Crystal Structure of SUMO-3-modified Thymine-DNA Glycosylase. *J. Mol. Biol.* **359**, 137–147 (2006).

Methods

Protein expression and purification

Proteins were prepared as described previously[18,20,35]. Protein purification buffers and columns used are provided in Supplementary Table 1. His-TEV-USP1$^{\Delta 1\text{-}66,\Delta 125\text{-}138,\Delta 229\text{-}408,\Delta 608\text{-}737}$-UAF1$^{\Delta 564\text{-}677}$ (USP1$^{\Delta N\Delta 1\Delta 2}$-UAF1$^{\Delta SLD}$) was co-expressed and His$_6$-TEV-USP1^{G670A,G671A}, His$_6$-TEV-USP1^{G670A,G671A,C90S}, and His$_6$-TEV-UAF1$^{27\text{-}359}$ (β-propeller domain) were expressed in *Sf*21 insect cells. Cells were lysed by sonication, clarified, and purified by Ni-NTA affinity then anion exchange chromatography. Subsequently, TEV protease treatment was performed overnight at 1:10 protease to target protein with gentle agitation before subtractive Ni-NTA affinity chromatography. Flow-through was concentrated to ~10 mg/mL and separated by gel filtration. Purified protein was concentrated to 5-15 mg/mL and stored at -80°C in 10-20 µL single-use aliquots. All steps were performed on ice or at 4°C and completed within 24-36 hours of lysis. Propargylated ubiquitin was prepared from a ubiquitin-intein-CBD construct via reaction with MESNa then propargylamine at 4°C as described previously[20]. USP1$^{\Delta N\Delta 1\Delta 2}$-UAF1$^{\Delta SLD}$ (80 µM) was incubated with propargylated ubiquitin (240 µM) for 30 min at room temperature in 50 mM Tris pH 7.5, 120 mM NaCl, 10 mM DTT. The crosslinked complex (USP1$^{\Delta N\Delta 1\Delta 2\text{-}Ub\text{-}prg}$-UAF1$^{\Delta SLD}$) was then purified by gel filtration (Superdex 200 Increase 10/300 GL; 20 mM Tris pH 8.0, 100 mM NaCl, 5% glycerol, 10 mM DTT).

His$_6$-3C-UAF1, His$_6$-TEV-UAF1$^{2\text{-}580}$ (UAF1$^{\Delta SLD}$), His$_6$-3C-FANCD2, His$_6$-FANCI, His$_6$-TEV-V5-FANCI, and His$_6$-TEV-V5-FANCI mutants were prepared as above with the exclusion of the TEV protease treatment and subtractive Ni-NTA affinity steps. FANCD2 was ubiquitinated and purified using an engineered Ube2T and SpyCatcher-SpyTag setup described in detail elsewhere[35,36]. For FANCD2, the His$_6$-3C tag was removed by 3C protease treatment during preparation of the mono-ubiquitinated version. For FANCI mutants in which the His$_6$-tag of FANCI was removed, overnight TEV protease treatment and subtractive Ni-NTA was performed prior to gel filtration.

Protein concentrations were determined using the predicted extinction coefficients at 280 nm[43] and absorbance via a Nanodrop. The ratio of 260nm/280nm was ≤0.65 for all protein batches used in subsequent experiments.

Crystallization, data collection, and processing

Crystals used to solve the structures were grown by hanging drop at 19°C. Purified USP1$^{\Delta N\Delta 1\Delta 2}$-UAF1$^{\Delta SLD}$ was concentrated to 11-15 mg/mL and drops of 4.5 µL were setup using a reservoir of 10% w/v PEG4000, 100 mM MES/Imidazole pH 6.0-6.5, 30 mM $CaCl_2$, 30 mM $MgCl_2$, 20-25% glycerol v/v and a ratio of 2 volumes protein to 1 volume reservoir. Purified USP1$^{\Delta N\Delta L1\Delta L2}$-UAF1$^{\Delta SLD}$ was reacted with propargylated ubiquitin (USP1$^{\Delta N\Delta 1\Delta 2\text{-Ub-prg}}$-UAF1$^{\Delta SLD}$) was concentrated to 4-7 mg/mL and drops of 3-4.5 µL were setup using a reservoir of 8-13% w/v PEG3350, 0.1 M citric acid/Bis-Tris propane pH 4.1 and a ratio of 2 volumes protein to 1 volume reservoir. For cryo-protection, crystals were transferred into reservoir solution supplemented with 25% glycerol and incubated for 5 min up to 12 hours, followed by vitrification in liquid nitrogen.

X-ray diffraction data were collected on a PILATUS 6M-F detector at Diamond Light Source, Beamline I04, using a wavelength of 0.9795 Å with crystals maintained at approximately 100 K. For USP1$^{\Delta N\Delta L1\Delta L2\text{-Ub-prg}}$-UAF1$^{\Delta SLD}$, indexing and integration were performed using iMosflm[44], and scaling and merging using AIMLESS[45]. For USP1$^{\Delta N\Delta L1\Delta L2}$-UAF1$^{\Delta SLD}$ diffraction was anisotropic and was processed using the STARANISO web server (http://staraniso.globalphasing.org/cgi-bin/staraniso.cgi). The resulting resolutions were 4.312 Å in the 0.902 a* + 0.433 b* direction, 4.381 in the 0.879 a* + 0.476 b* direction, and 3.601 in the 0.246 a* + 0.469 b* + 0.848 c* direction. For USP1$^{\Delta N\Delta 1\Delta 2\text{-Ub-prg}}$-UAF1$^{\Delta SLD}$, molecular replacement was performed using PHASER[46], with PDB 5CVN[25] chain B (with side chains removed) and 5CVL[25] used as search models for USP1 and UAF1 respectively. One USP1 molecule and two UAF1 molecules were placed. Strong positive difference density for the Zn atom in the USP1 fingers

subdomain was used to validate the molecular replacement solution. Iterative manual modeling building and automated refinement were performed using COOT[47] and Refmac5[48], respectively. During automated refinement UAF1 from PDB 51KA[23] (chain B) was used to provide reference restraints. After several rounds of refinement, another USP1 molecule and two ubiquitin molecules were placed using rigid body fitting. For USP1$^{\Delta N\Delta 1\Delta 2}$-UAF1$^{\Delta SLD}$, molecular replacement was performed using USP1$^{\Delta N\Delta 1\Delta 2\text{-Ub-prg}}$-UAF1$^{\Delta SLD}$ chains A and B, and refined as above. Final refinement steps were performed in phenix[49]. Crystallography data and model statistics are reported in Table 1. For the USP1$^{\Delta N\Delta 1\Delta 2}$-UAF1$^{\Delta SLD}$ structure 93.79% of residues were within allowed regions of the Ramachandran plot and 0.51% of residues in outlier regions. For the SP1$^{\Delta N\Delta 1\Delta 2\text{-Ub-prg}}$-UAF1$^{\Delta SLD}$ structure 95.91% of residues were within allowed regions of the Ramachandran plot and 0.31% of residues in outlier regions.

SAXS data collection and processing

Size-exclusion chromatography (SEC) coupled to SAXS measurements were performed at the Diamond Light Source, Beamline B21 via the mail-in service. USP1$^{\Delta N\Delta 1\Delta 2\text{-Ub-prg}}$-UAF1$^{\Delta SLD}$ at ~10 mg/mL was thawed and injected at 0.075 mL/min onto a Superose 6 Increase 3.2/300 column equilibrated with 20 mM Tris pH 8.0, 200 mM NaCl, 5% glycerol, 5 mM DTT. SAXS data were collected on an Eiger 4M detector. Buffer subtraction and averaging were performed using chromixs[50]. Buffer subtracted, averaged scattering was analyzed using ATSAS[50] and RAW[51]. Crysol was used to fit PDB models to the SAXS data.

Gel filtration analysis

To prepare the USP1^{C90S}-UAF1-FANCI-FANCD2^{Ub} complex the four individually purified subunits were thawed on ice and mixed 1.2:1.2:1:1. The assembled complex was diluted to ~5 mg/mL and a total volume of 250 µL with 20 mM Tris pH 8.0, 25 mM NaCl, 5% glycerol, 3 mM MgCl2, 1 mM DTT to yield a final NaCl concentration of approximately 200 mM. The sample was then injected at 0.5 mL/min onto a

Superose 6 Increase GL 10/300 column equilibrated in EM buffer (20 mM Tris pH 8.0, 150 mM NaCl, 2 mM DTT).

Cryo-EM sample preparation and data collection

The USP1^{C90S}-UAF1-FANCI-FANCD2^{Ub} complex was prepared by mixing the four individually purified subunits 1:1:1:1. The complex was exchanged into EM buffer using a Bio-Spin P-30 column (Bio-Rad). The concentration of complex was estimated from absorbance at 280 nm and 1 equivalent of dsDNA (61 base pairs; TGATCAGAGGTCATTTGAATTCATGGCTTCGAGCTTCATGTAGAGTCGACGGTGCTGGGAT; IDT) per protein complex was added. Immediately prior to preparing grids the sample was equilibrated to room temperature for 5 min. Quantifoil 1.2/1.3 300 mesh grids were glow discharged twice and 3.6 µL of at 8.8 µM complex was applied. The grids were blotted for 2.5 s and vitrified in liquid ethane using a Vitrobot operating at ~95% humidity at 15°C.

Cryo-EM data collection and processing

A CRYO ARM 300 (JEOL) equipped with a DE64 detector was used to collect a total of 4912 movies using beam-Image shift at the Scottish Centre for Macromolecular Imaging (SCMI). All movies were collected in counting mode with a calibrated pixel size of 1.015 Å using SerialEM[52]. Movies were as 59 frames for a total dose of ~65 $e^-/Å^2$ over 14.9 s. A subset of the movies were additionally gain corrected using relion_estimate_gain[53]. Subsequent processing was performed in Cryosparc v2.13.2[54] (Extended Data Fig. 2-3). Patch motion correction, patch CTF estimation, and manual curation was performed resulting in 4593 dose-weighted, motion corrected images. Blob picking was performed with minimum and maximum particle diameters of 100 Å and 220 Å respectively, using an elliptical blob. 2D classification was used to generate classes for template picking and select particles for *ab initio* reconstruction with 4 classes, from which a single class with clear secondary structure features was obtained. Template picking was performed on the entire dataset and 1,485,510 boxes were extracted at a box size of 300

pixels (Extended Data Fig. 3). To remove non-particles, multiple rounds of heterogenous refinement were performed with one good starting model and 2 or 3 "junk" starting models not representing the protein complex of interest, all low pass filtered to 20 Å. Following this, local motion correction and re-extraction of particles at a box size of 320 pixels were performed. A further round of heterogenous refinement was performed using the same starting model low-pass filtered at 12 Å, 15 Å, 20 Å, and 30 Å. This resulted in 249,732 particles in the highest resolution class. This particle set was used for homogeneous refinement, followed by non-uniform, local refinement using the dynamic mask generated from homogenous refinement[55]. The resulting masked map gave a global resolution of 3.7 Å at a Fourier Shell Correlation (FSC) threshold of 0.143 (Extended Data Fig. 2d)[55]. 3D variability analysis was performed using a filter resolution of 4.2 Å and solving for 3 modes[38].

The local resolution was estimated using FSC threshold of 0.5 and Adaptive Window Factor of 6, which was then used for local filtering (Extended Data Fig. 2e). DeepEMhancer (version 0.13)[56], via the COSMIC2 web platform (https://cosmic-cryoem.org/)[57], was used to post-process the half-maps using the highRes learning model to aid interpretation.

Model building

Initially rigid body fitting was performed with USP1 and ubiquitin from the ubiquitin-free structure (chains A and C), UAF1 from PDB 5K1A[25] (chain B), and FANCI and FANCD2 from PDB 6VAF[15] (chains A and B) using UCSF Chimera[58]. The N-terminal region of FANCD2 (residues 45 to 311) was fitted as a rigid body into the locally filtered map[47]. Manual model editing was performed using COOT and incorporating torsion, planar peptide, trans peptide, and Ramachandran restraints. Where appropriate, secondary structure restraints were also included. Automated refinement against a globally sharpened map, with the B-factor estimated from the Guinier plot, was performed using phenix real-space refinement[59]. A non-bonded weight of 250 was used to reduce steric clashes and a refinement resolution of 4.1 Å

(FSC=0.5). Bond and angle restraints for the USP1 Zinc finger and the K561-G76 isopeptide bond were incorporated. UAF1 from PDB 51KA (chain B) was used to provide reference restraints. The dsDNA was modelled using rigid body fitting of chains S and T from PDB 6VAE[15]. Following refinement the DNA was stubbed as the local resolution was insufficient to assign the sequence. Cryo-EM data and model statistics are reported in Table 2. The FSC between the model and map (FSC_{full}) was computed using phenix[49] (Extended Data Fig. 2f). The FSC_{work} and FSC_{free} were computed by first introducing a random 0.3 Å shift in the refined model coordinates using *phenix.pdbtools*, followed by refinement against the first half-map (sharpened with *phenix.auto_sharpen* – no reference model), and finally calculation of the FSC between the re-refined model and the first half-map (FSC_{work}) and the second half-map (FSC_{free}) (Extended Data Fig. 2f).

Superposition of atomic models was performed using "MatchMaker" in UCSF Chimera with the default settings unless otherwise specified. Rotations were estimated using the "measure rotation" command in UCSF Chimera. Buried surface area calculations were performed using PISA[60]. Structures were analysed using UCSF Chimera[58], ChimeraX[61], or PyMOL (The Molecular Graphics System, Version 1.8, Schrödinger, LLC). Figures were produced with UCSF Chimera[58] or ChimeraX[61].

Deubiquitination assays

Deubiquitination reactions were performed by preparing a 2x substrate mix and a 2x enzyme mix, and mixing these 1:1 to initiate the reaction. Both mixes were setup on ice, and then incubated at room temperature 30 min prior to reaction initiation and during the reaction. 5 µL aliquots of the reaction were terminated at the indicated timepoints by addition of 5 µL 2x NuPAGE LDS buffer (Thermo Fisher) supplemented with 200 mM DTT.

The 2x substrate mixes were prepared by diluting stocks (≥30 µM) of $FANCD2_{Ub}$, His_6-V5-TEV-FANCI (or matched buffer), and dsDNA (61 base pairs) with DUB buffer (20 mM Tris pH 8.0, 75 mM NaCl, 5%

glycerol, 1 mM DTT). The resulting 2x mixes were composed 2 µM FANCD2$_{Ub}$, 2 µM FANCI, 8 µM dsDNA. The 2x enzyme mixes were prepared by diluting concentrated stocks (≥30 µM) of USP1, and UAF1 (full-length or β-propeller domain) with DUB buffer. The resulting 2x mixes were composed of 200 nM USP1 and 200 nM UAF1 (full-length) or 400 nM USP1 and 400 nM UAF1 (β-propeller domain). SDS-PAGE, Coomassie staining, and western blotting was performed as described previously[18]. For western blotting, 1:1000 dilution Rabbit Anti-FANCD2 (ab108928) and 1:8000 dilution Mouse Anti-V5 (ab27671) were used for detection of FANCD2 and FANCI, respectively. Secondary antibodies labeled with IRDye 680RD or 800CW (Donkey anti-rabbit IgG or anti-mouse IgG; Li-Cor) were used at 1:10,000 dilution. Bands were subsequently visualized on an Odyssey CLX Infrared Imaging System (Li-COR). Each band was quantified using Image Studio with horizontal background subtraction (Li-COR). Percentage ubiquitination was calculated from the ratio of the ubiquitinated band to the sum of the non-ubiquitinated and ubiquitinated bands. Replicate assays were performed from different thawed protein aliquots, each from the same protein preparation. Plots were prepared using matplotlib[62].

Microscale Thermophoresis assays

FANCI mutants with the His$_6$-tag removed (V5-FANCI^{S556A,S559A,S565A} or V5-FANCI^{S556D,S559D,S565D}) were exchanged into MST buffer 1 (20 mM Tris pH 8.0, 150 mM NaCl, 5% glycerol, 0.47 mg/mL BSA, 1 mM DTT) by 5-fold dilution with Dilution buffer (20 mM Tris pH 8.0, 87.5 mM NaCl, 5% glycerol, 0.59 mg/mL BSA). Two-fold serial dilutions of exchanged protein were set up in PCR tubes with MST Buffer 1. His$_6$-3C-UAF1 (200 nM) was labeled with RED-tris-NTA dye (50 nM; Nanotemper) in MST buffer 2 (20 mM Tris pH 8.0, 50 mM NaCl, 5% glycerol, 0.47 mg/mL BSA, 1 mM DTT) and added 1:1 to the serial dilution of FANCI mutants. This resulted in measurement conditions of 100 nM His$_6$-3C-UAF1 and 25 nM dye in 20 mM Tris pH 8.0, 100 mM NaCl, 5% glycerol, 0.47 mg/mL BSA, 1 mM DTT. Prior to MST measurement samples were briefly centrifuged then transferred into premium capillaries (NanoTemper Technologies). Measurements were performed at 22 °C on a Monolith NT.115 instrument (NanoTemper Technologies)

669 using the red channel and a laser power of 60%. MST traces between 0.5 and 1.5 seconds were
670 quantified using MO.Affinity Analysis v2.3. Estimation of dissociation constants was not performed as
671 saturation was not reached. Plots were prepared using matplotlib[62].

672

673 **Data availability**

674 The atomic coordinates and structure factors of ubiquitin-free and ubiquitin-bound USP1-UAF1
675 have been deposited to the PDB with accession codes PDB 7AY0 and PDB 7AY2, respectively.
676 The atomic coordinates and cryo-EM maps, including locally filtered and sharpened and
677 DeepEMhancer maps, have been deposited to the PDB and EMDB with accession codes PDB
678 7AY1 and EMD-11934, respectively. Source data are available online.

679

680

Figure Legends

Figure. 1. Structural characterization of USP1-UAF1. (**a**) Crystal structure of USP1, lacking the NTE and Insert 1 and Insert 2, in complex with UAF1 lacking the SLD. Subdomains of USP1 and domains of UAF1 are indicated. Deleted regions are indicated in the primary structure as dashed lines (see also Methods). (**b**) Crystal structure of USP1 lacking the N-terminal region and Insert 1 and Insert 2 covalently modified with propargylated ubiquitin in complex with UAF1 lacking the SLD. The termini and approximate positions where the NTE, Insert 1, and Insert 2 would be are indicated. The rotation axis relating the palm and thumbs of the two structures is shown. (**c**) The interface between the fingers of USP1 and the β-propeller of UAF1. Side chains involved in salt bridges are highlighted. (**d**) Fit of the ubiquitin-bound crystal structure with solution state SAXS measurements. (**e**) Comparison of USP1 catalytic region between the ubiquitin-free (gray) and ubiquitin-bound (colored) crystal structures. Structures were aligned by the USP1 subunit.

Figure. 2. Structural characterization of full-length USP1-UAF1 bound to the FANCI-FANCD2^{Ub} substrate. (**a**) Locally filtered cryo-EM map of the complex containing USP1 (pink), UAF1 (orange), FANCI (violet), and ubiquitinated (yellow) FANCD2 (green) at a threshold of 0.4. (**b**) Model of the enzyme-substrate complex. (**c**) The catalytic site of USP1 with the FANCD2^{K561}-ubiquitin^{G76} isopeptide linkage overlaid with the DeepEMhancer[56] map at a threshold of 0.1. The Cα trace and side chains are shown. Hydrogen bonds are shown as black dashed lines.

Figure. 3. FANCI-UAF1 interactions are important for deubiquitination of FANCI-FANCD2^{Ub}. (**a**) The interface between FANCI (violet) and UAF1 (orange). The interface spans UAF1 but does not include the previously predicted SLIM (bottom left). The FANCI$^{249-260}$ loop inserts into the hydrophobic pocket of the SLD of UAF1 (top right), while the FANCI$^{547-576}$ region interacts with the β-propeller domain of UAF1 (bottom right). Hydrophobic side chains involved in the interaction are shown and potential backbone hydrogen bonds are highlight as black dashed lines. (**b**) Truncations of UAF1 reduce FANCI-FANCD2^{Ub} deubiquitination. Deubiquitination of FANCD2^{Ub} (1 μM) in complex with non-ubiquitinated FANCI (1 μM) by full-length USP1 reconstituted with UAF1 or truncations of UAF1 (200 nM enzyme complex) was assessed by SDS-PAGE and Coomassie staining (see also Extended Data Fig. 5). Assays were in the presence of 4 μM 61 base pair dsDNA, and performed twice (two technical replicates). (**c**) Phosphorylation within FANCI$^{547-576}$ regulates deubiquitination. Deubiquitination of FANCD2^{Ub} (1 μM) in complex with non-ubiquitinated FANCI phosphorylation mimics (1 μM) by full-length USP1 reconstituted

with full-length UAF1 (100 nM enzyme complex) was assessed using SDS-PAGE and Coomassie staining. Assays were in the presence of 4 μM 61 base pair dsDNA, and performed twice (two technical replicates). Uncropped gels in panel b and c are provided as Source Data.

Figure. 4. Conformational changes in FANCI (green) and FANCD2 (violet) during the deubiquitination cycle. (**a**) Conformational changes of ubiquitin (yellow) associated with USP1-UAF1 binding. Structures of the deubiquitination substrate FANCI-FANCD2^{Ub} (PDB 6VAF) and the deubituitination product FANCI-FANCD2 (PDB 6VAD)[15] were aligned to the USP1-UAF1-FANCI-FANCD2^{Ub} structure by the FANCI subunit. The axis of rotation for ubiquitin is shown as a black cylinder and I44 of ubiquitin represented as spheres. In the deubiquitinated state (bottom panel) FANCD2 and USP1 would sterically clash. (**b**) Aligned FANCD2 subunits from FANCI-FANCD2^{Ub} (PDB 6VAF[15]; dark gray), USP1-UAF1-FANCI-FANCD2^{Ub} (green), and FANCI-FANCD2 (PDB 6VAD[15]; light gray). The N-terminus of FANCD2 in the USP1-UAF1-FANCI-FANCD2^{Ub} structure (locally filter map at a threshold of 0.15) is in an intermediate conformation between the FANCI-FANCD2^{Ub} and FANCI-FANCD2 states. (**c**) Aligned FANCI subunits from FANCI-FANCD2^{Ub} (dark gray), USP1-UAF1-FANCI-FANCD2^{Ub} (violet), and FANCI-FANCD2 (light gray). Although all three states are globally very similar, FANCI of USP1-UAF1-FANCI-FANCD2^{Ub} more closely resembles the non-ubiquitinated FANCI-FANCD2 state in the region close to the UAF1 interface.

Figure. 5. Schematic representation of the deubiquitination cycle of FANCI-FANCD2 by USP1-UAF1. The flexible USP1-UAF1 enzyme complex (E) binds the FANCI-FANCD2^{Ub} substrate (S) to form the enzyme substrate complex (ES) in which ubiquitin is extracted from its interaction with FANCI. Upon cleavage of the isopeptide bond between FANCD2 and ubiquitin the FANCI-FANCD2 complex (P) presumably dissociates from the USP1-UAF1-ubiquitin complex (EP) first, followed by ubiquitin. Key regulatory features of the reaction are highlighted.

Tables

Table 1. Crystallography data collection and model refinement statistics[a]

	Ubiquitin-free (PDB 7AY0)	Ubiquitin-bound (PDB 7AY2)
Data collection		
Space group	$P4_1$	$P6_5$
Cell dimensions		
a, *b*, *c* (Å)	119.57, 119.57, 195.46	134.24, 134.24, 274.67
α, β, γ (°)	90, 90, 90	90, 90, 120

Resolution (Å)	84.549-3.602 (3.754-3.602)	91.56 – 3.20 (3.31 – 3.20)
R_{pim}	0.108 (0.727)	0.059 (0.519)
R_{meas}	0.258 (1.698)	0.193 (1.657)
$I / \sigma I$	6.4 (1.7)	11.6 (1.7)
$CC_{1/2}$	0.992 (0.565)	0.997 (0.581)
Completeness (spherical, %)	80.3 (34.2)	100 (100)
Completeness (ellipsoidal, %)[b]	95.0 (100)	-
Redundancy	5.7 (5.4)	10.5 (10.1)
Refinement		
Resolution (Å)	56.78 – 3.60	67.12 – 3.20
No. reflections	25,467	46,045
R_{work} / R_{free}	0.235 / 0.266	0.204 / 0.234
No. atoms		
Protein	12,747	13,445
Ligand/ion	2	6
Water	0	0
Mean *B*-factors (Å^2)		
Protein	86.6	98.7
Ligand/ion	69.3	89.1
Water	-	-
R.m.s. deviations		
Bond lengths (Å)	0.003	0.004
Bond angles (°)	0.808	0.909

[a]Values in parentheses are for highest-resolution shell. Each structure is from a single crystal.
[b]Anisotropy analyzed using the STARANISO web server, see Methods.

Table 2. Cryo-EM data collection and model refinement and validation statistics

	USP1-UAF1-FANCI-FANCD2^{Ub} (EMD-11934, PDB 7AY1)
Data collection and processing	
Magnification	120,000x
Voltage (kV)	300
Electron exposure (e–/Å^2)	65
Defocus range (μm)[a]	0.22 – 3.7
Pixel size (Å)	1.015
Symmetry imposed	C1
Initial particle images (no.)	1,485,510
Final particle images (no.)	249,732
Map resolution (Å)[b]	3.7
FSC threshold	0.143
Map resolution range (Å)[c]	3.4 – 9.9
Refinement	
Initial model used (PDB code)	6VAF[15], 5K1A[23], 7AY2 (ubiquitin-bound USP1)
Model resolution (Å)	3.7
FSC threshold	0.143

Model resolution range (Å)	3.4 – 9.9
Map sharpening *B* factor (Å^2)	76.9
Model composition	
Non-hydrogen atoms	25186
Protein residues	3080
Nucleotide residues	58
Ligands/ions	1
Mean *B* factors (Å^2)	
Protein	58.5
Ligand/ions/nucleotides	343.1
R.m.s. deviations	
Bond lengths (Å)	0.008
Bond angles (°)	1.009
Validation	
MolProbity score	1.73
Clashscore	6.81
Poor rotamers (%)	0.04
Ramachandran plot	
Favored (%)	94.80
Allowed (%)	5.14
Disallowed (%)	0.07

741 [a]Based on CTF fitting.
742 [b]After FSC-mask auto-tightening in Cryosparc.
743 [c]1% to 99% quantiles from local resolution map.
744

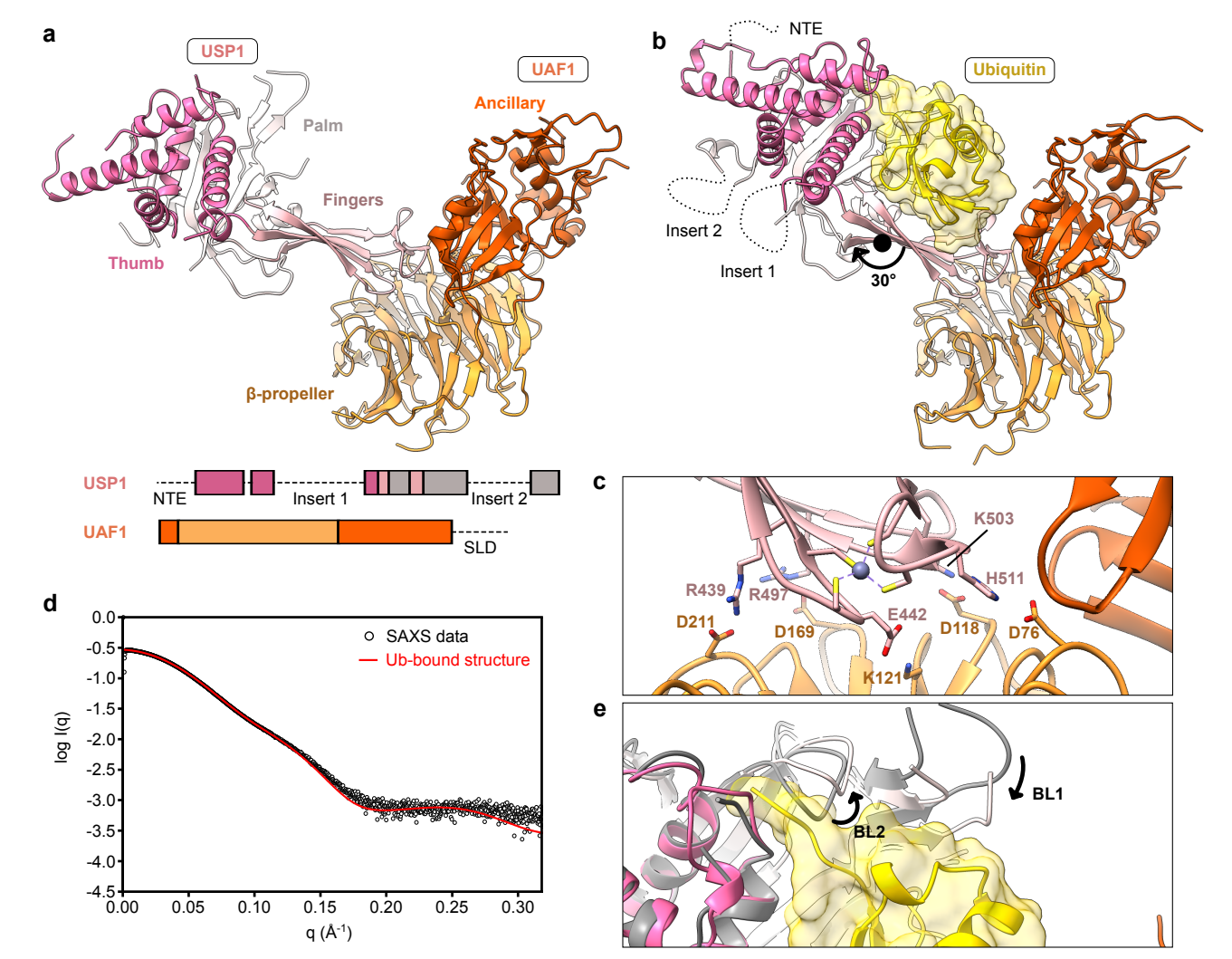
a
USP1
UAF1
Ancillary
Palm
Fingers
Thumb
β-propeller
b
NTE
Ubiquitin
Insert 2
Insert 1
30°
USP1
NTE
Insert 1
Insert 2
UAF1
SLD
c
K503
H511
R439
R497
E442
D211
D169
D118
D76
K121
d
SAXS data
Ub-bound structure
log I(q)
q (Å-1)
e
BL1
BL2

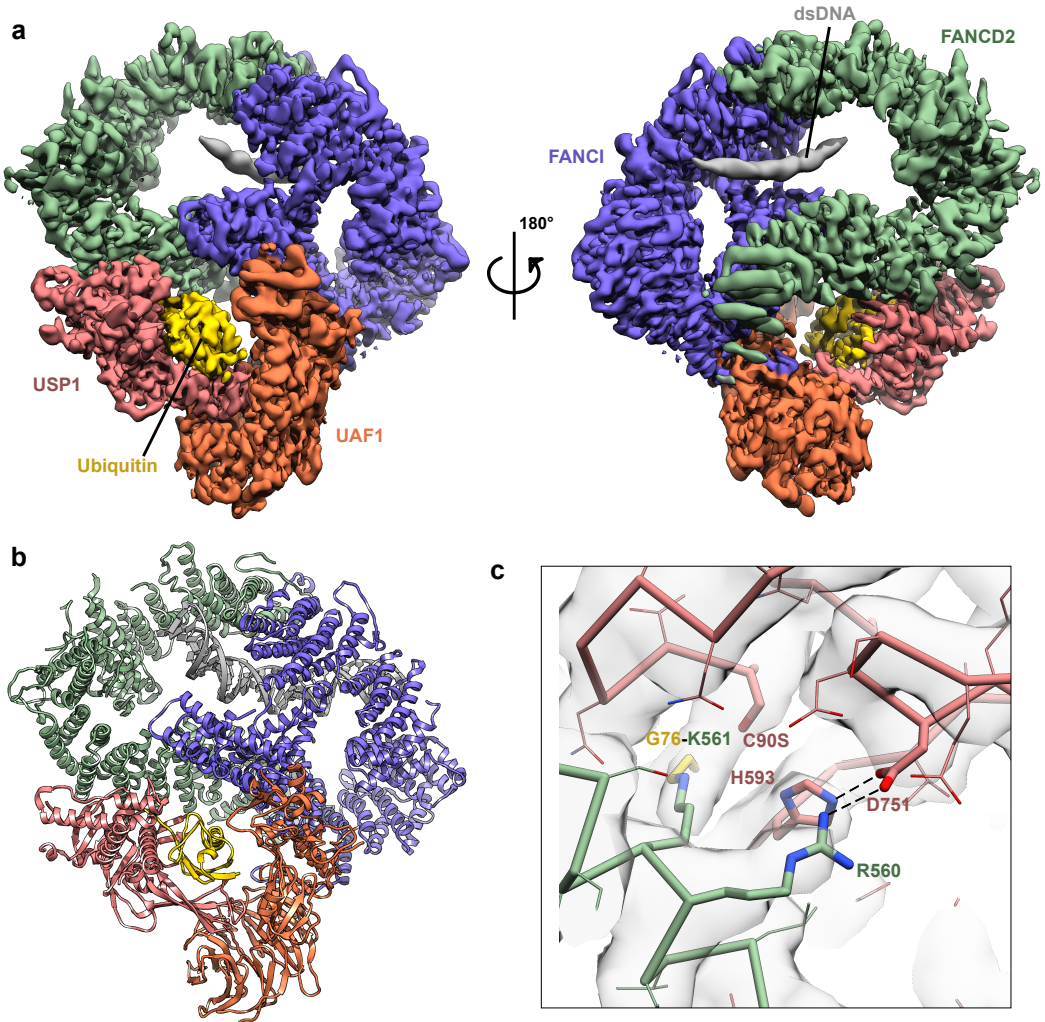
a
dsDNA
FANCD2
FANCI
180°
USP1
UAF1
Ubiquitin
b
c
G76-K561
C90S
H593
D751
R560

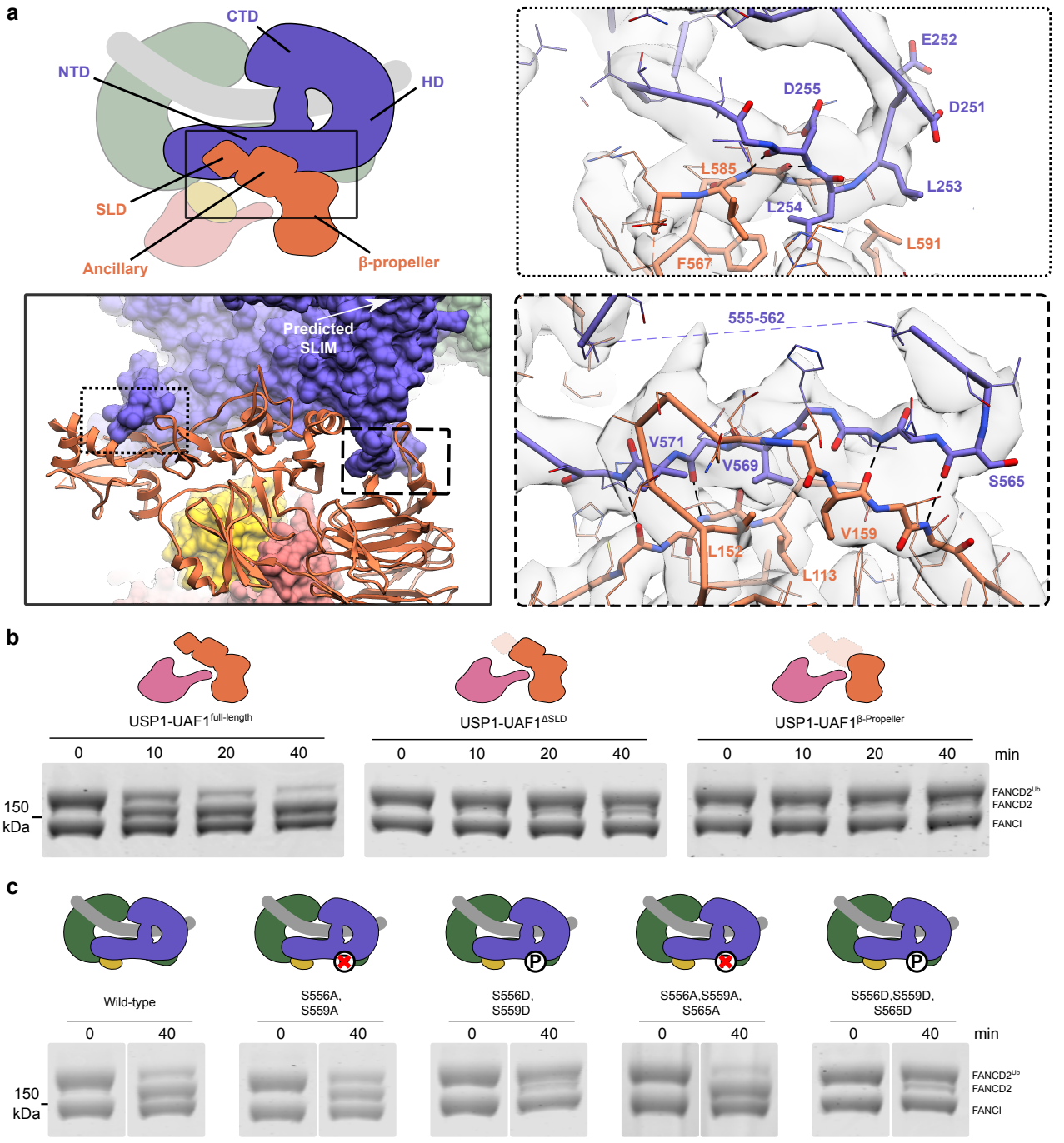
a
CTD
NTD
HD
SLD
Ancillary
β-propeller
E252
D255
D251
L585
L253
L254
L591
F567
Predicted
SLIM
555-562
V571
V569
S565
V159
L152
L113
b
USP1-UAF1full-length
USP1-UAF1ΔSLD
USP1-UAF1β-Propeller
0
10
20
40
min
150
kDa
FANCD2Ub
FANCD2
FANCI
c
Wild-type
S556A,
S559A
S556D,
S559D
S556A,S559A,
S565A
S556D,S559D,
S565D
P
0
40
min
150
kDa
FANCD2Ub
FANCD2
FANCI

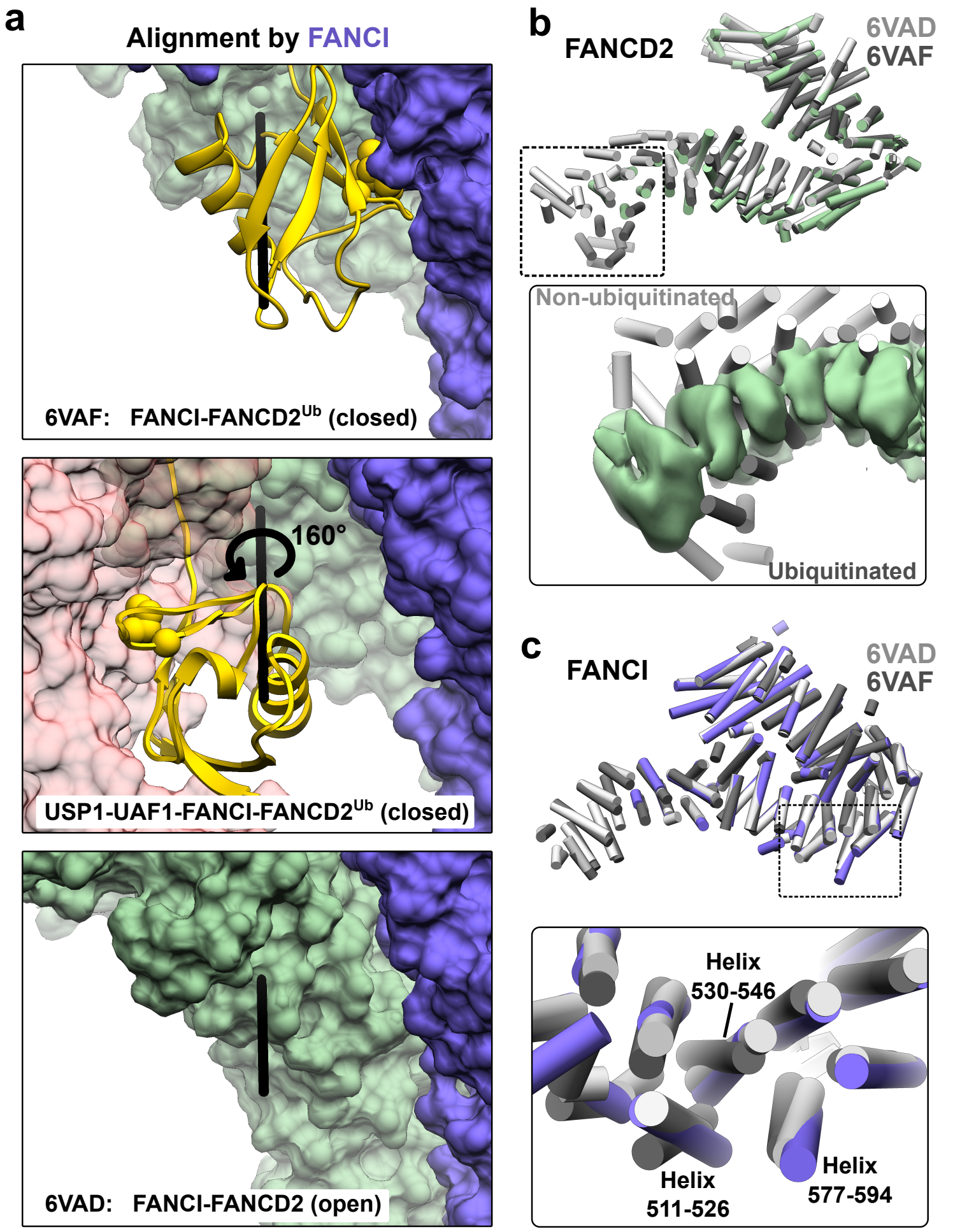
a
Alignment by FANCI
6VAF: FANCI-FANCD2Ub (closed)
160°
USP1-UAF1-FANCI-FANCD2Ub (closed)
6VAD: FANCI-FANCD2 (open)
b
FANCD2
6VAD
6VAF
Non-ubiquitinated
Ubiquitinated
c
FANCI
6VAD
6VAF
Helix
530-546
Helix
511-526
Helix
577-594

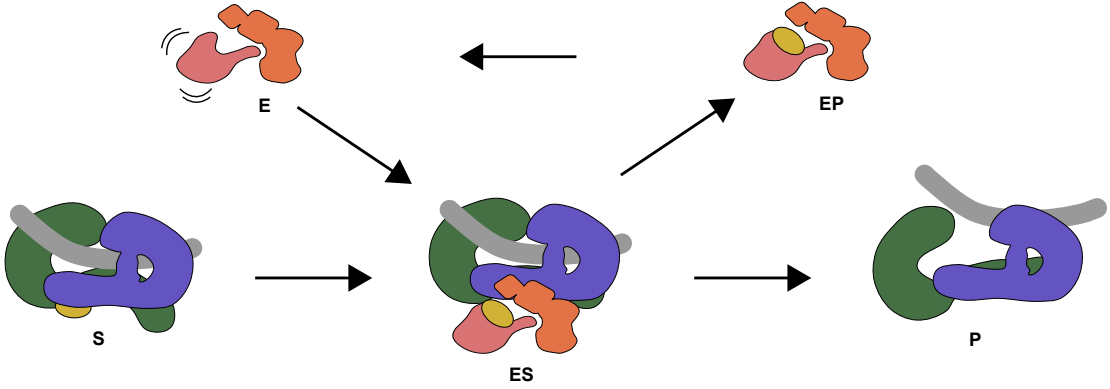

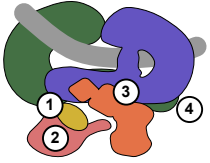

ES

① *Global substrate changes* (Ub)

② *Global and local enzyme changes* (USP1)

③ *Substrate adaption* (UAF1-FANCI)

Negative regulation (FANCI phosphorylation)

④ *Global substrate changes* (FANCD2)

Negative regulation (FANCI ubiquitination)

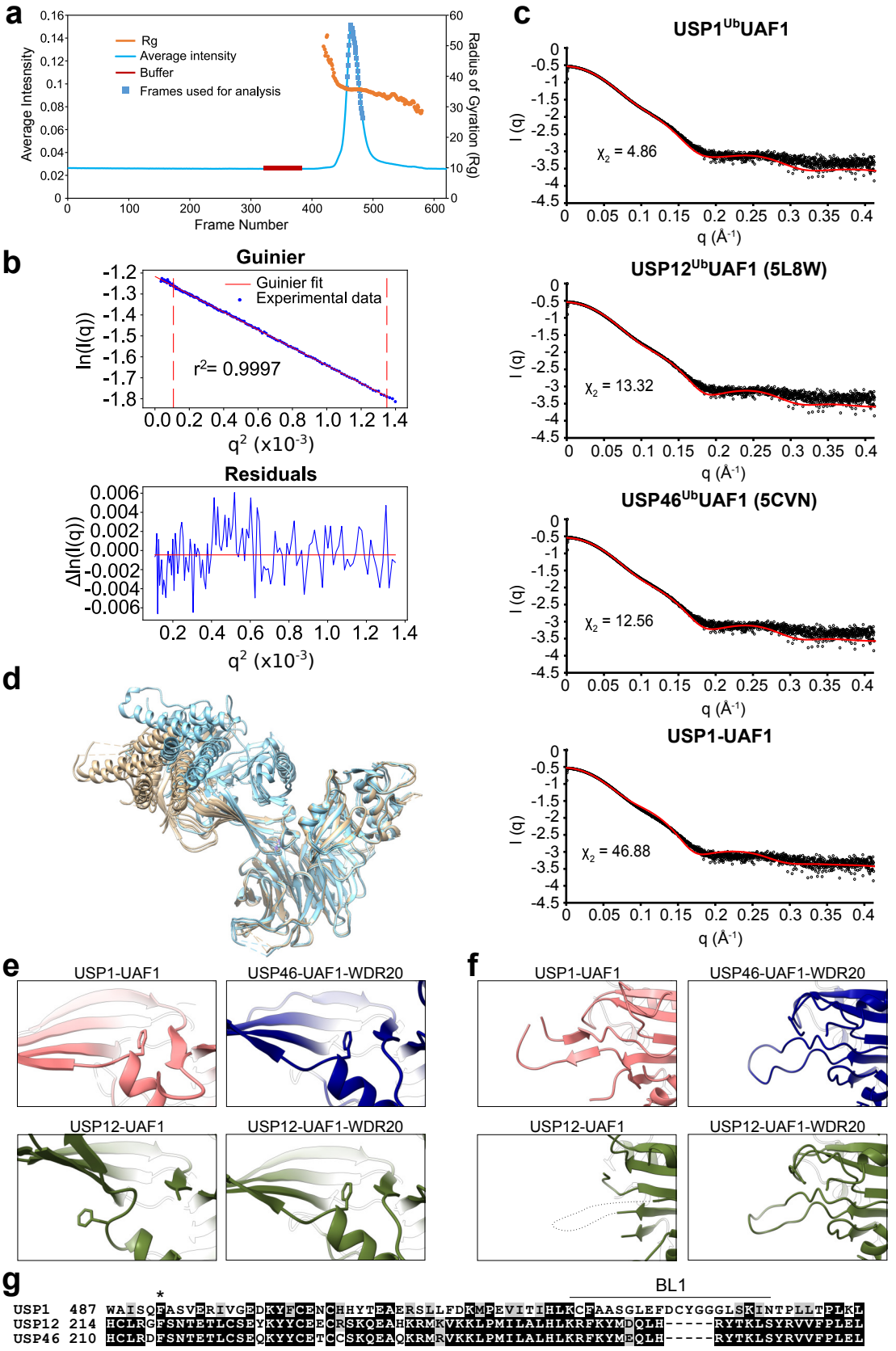
a
Rg
Average intensity
Buffer
Frames used for analysis
Average Intesnsity
Radius of Gyration (Rg)
Frame Number
b
Guinier
Guinier fit
Experimental data
r²= 0.9997
ln(I(q))
q² (x10⁻³)
Residuals
ΔIn(I(q))
q² (x10⁻³)
c
USP1^Ub UAF1
χ2 = 4.86
USP12^Ub UAF1 (5L8W)
χ2 = 13.32
USP46^Ub UAF1 (5CVN)
χ2 = 12.56
USP1-UAF1
χ2 = 46.88
I (q)
q (Å⁻¹)
d
e
USP1-UAF1
USP46-UAF1-WDR20
USP12-UAF1
USP12-UAF1-WDR20
f
USP1-UAF1
USP46-UAF1-WDR20
USP12-UAF1
USP12-UAF1-WDR20
g
BL1
USP1 487 WAISQFASVPRIVGPDKYFCENCHHYTEAERSLLFDKMPEVITIHLKCFAASGLEFDCYGGGLSKINTPLLTPLKL
USP12 214 HCLRGFSNTETLCSEYKYYCEECRSKQEAHKRMKVKKLPMILALHLKRFKYMDQLH-----RYTKLSYRVVFPLEL
USP46 210 HCLRDFSNTETLCSEQKYYCETCCSKQEAQKRMRVKKLPMILALHLKRFKYMEQLH-----RYTKLSYRVVFPLEL

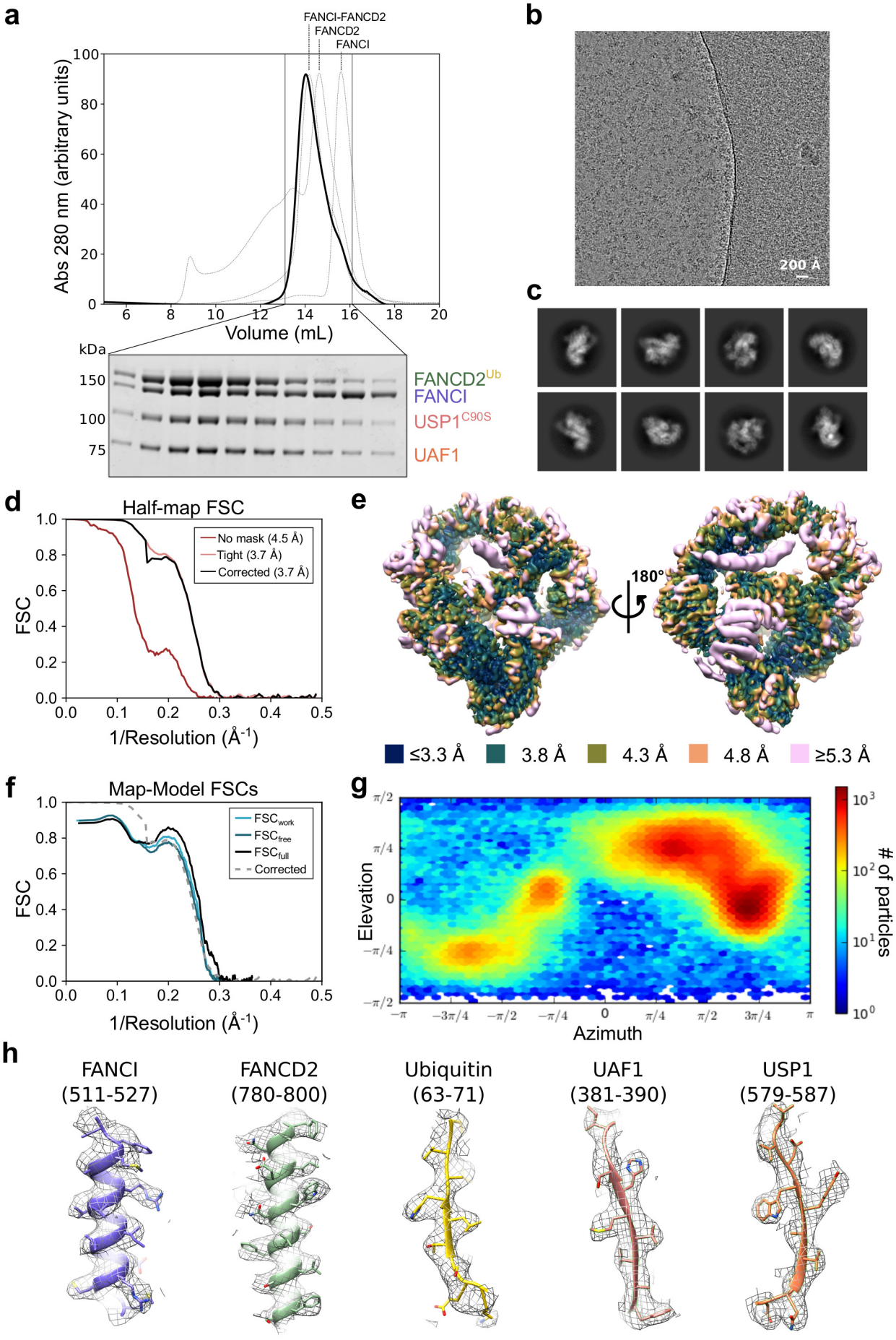
a
FANCI-FANCD2
FANCD2
FANCI
Abs 280 nm (arbitrary units)
Volume (mL)
kDa
150
100
75
FANCD2Ub
FANCI
USP1C90S
UAF1
b
200 Å
c
d
Half-map FSC
No mask (4.5 Å)
Tight (3.7 Å)
Corrected (3.7 Å)
FSC
1/Resolution (Å-1)
e
180°
≤3.3 Å
3.8 Å
4.3 Å
4.8 Å
≥5.3 Å
f
Map-Model FSCs
FSCwork
FSCfree
FSCfull
Corrected
FSC
1/Resolution (Å-1)
g
Elevation
Azimuth
# of particles
h
FANCI
(511-527)
FANCD2
(780-800)
Ubiquitin
(63-71)
UAF1
(381-390)
USP1
(579-587)

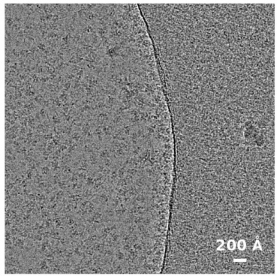

4,591 micrographs

Blob picking
2D classification
Template picking

1,486k particles

2D classification

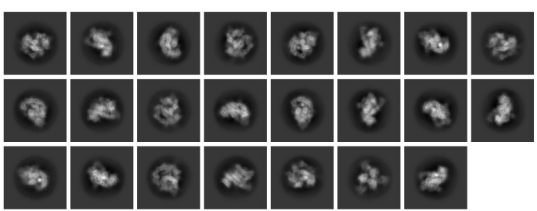

Ab initio model
reconstruction
(150k particles)

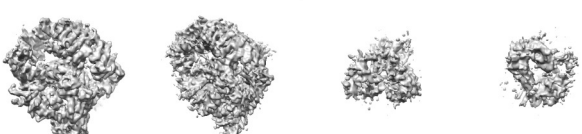

Heterogenous refinement
(multiple rounds)

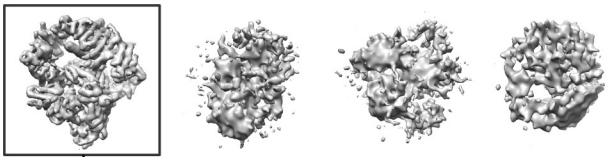

Local motion correction
Re-extraction 320px
Homogenous refinement

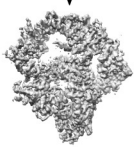

387k particles
4.0 Å

Heterogenous refinement
(sequentially filtered starting model)

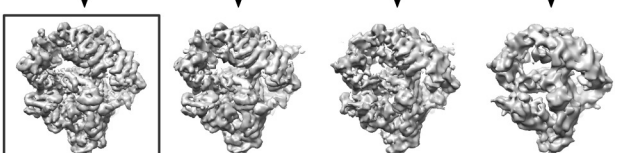

250k particles | 82k particles | 38k particles | 17k particles

Homogeneous refinement

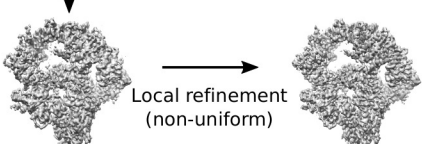

250k particles
3.9 Å

Local refinement
(non-uniform)

250k particles
3.7 Å

UAF1(SLD)-FANCI

SUMO3-TDG
(2D07)

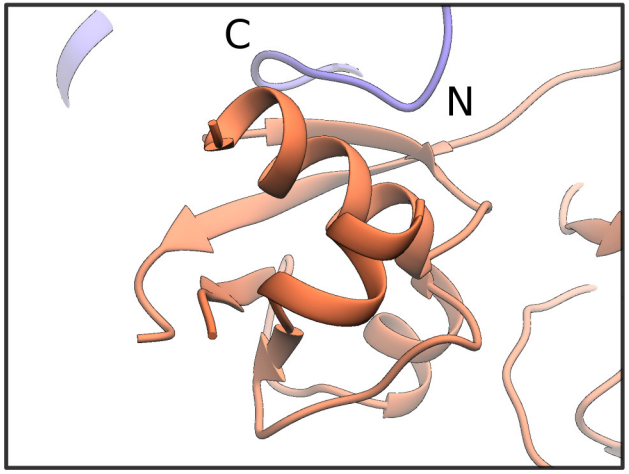

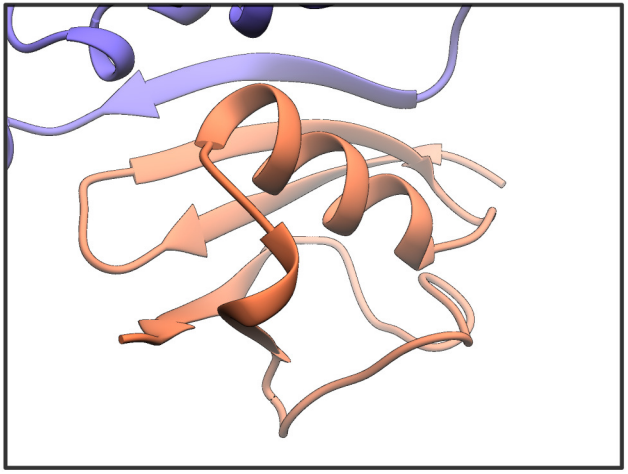

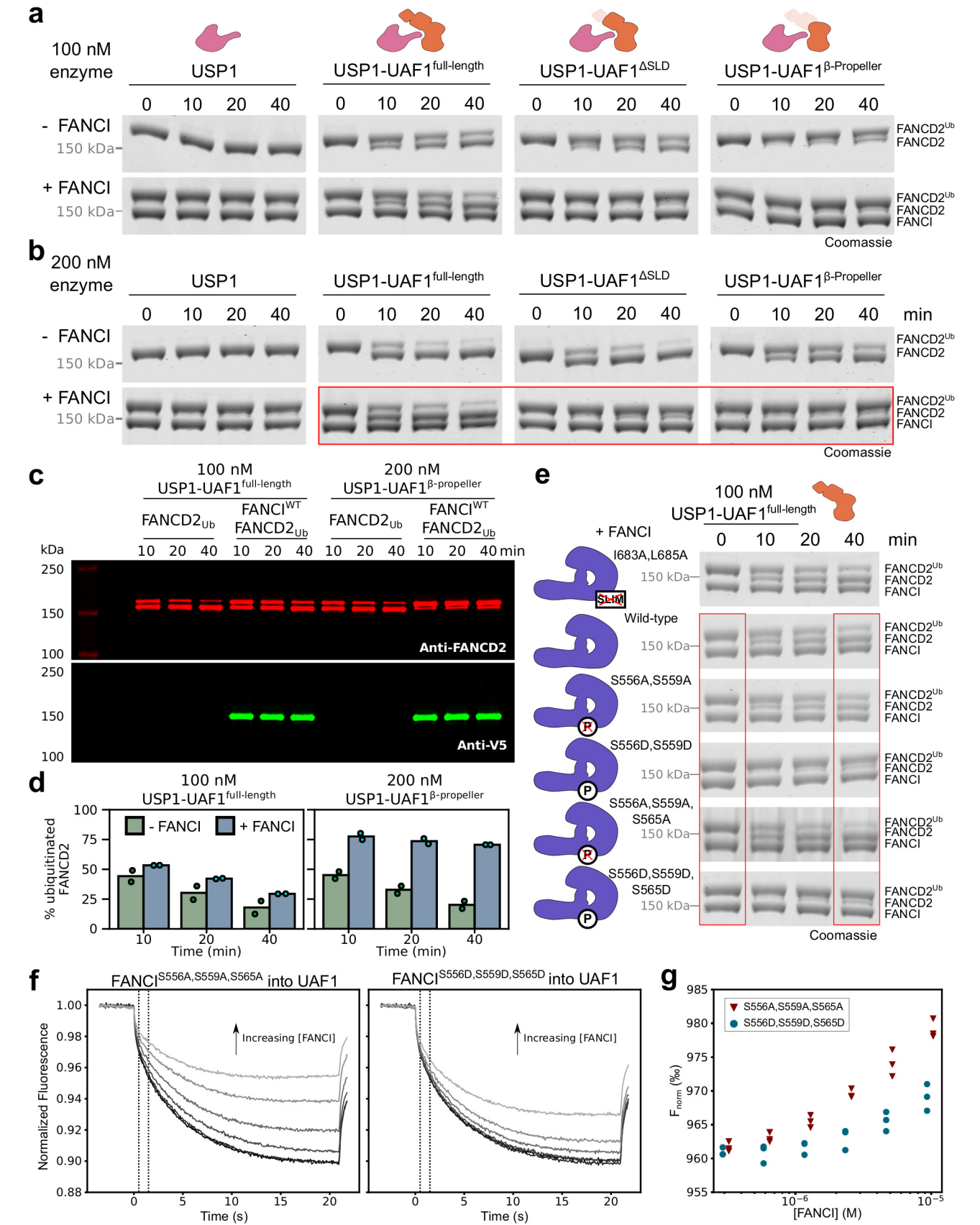
a
100 nM enzyme
USP1
USP1-UAF1full-length
USP1-UAF1ΔSLD
USP1-UAF1β-Propeller
0 10 20 40
- FANCI
+ FANCI
150 kDa
FANCD2Ub
FANCD2
FANCI
Coomassie
b
200 nM enzyme
min
c
100 nM USP1-UAF1full-length
200 nM USP1-UAF1β-propeller
FANCD2Ub
FANCIWT FANCD2Ub
kDa
250
150
100
Anti-FANCD2
Anti-V5
d
% ubiquitinated FANCD2
- FANCI
+ FANCI
Time (min)
e
+ FANCI
I683A,L685A
Wild-type
S556A,S559A
S556D,S559D
S556A,S559A, S565A
S556D,S559D, S565D
f
FANCIS556A,S559A,S565A into UAF1
FANCIS556D,S559D,S565D into UAF1
Increasing [FANCI]
Normalized Fluorescence
Time (s)
g
S556A,S559A,S565A
S556D,S559D,S565D
Fnorm (‰)
[FANCI] (M)

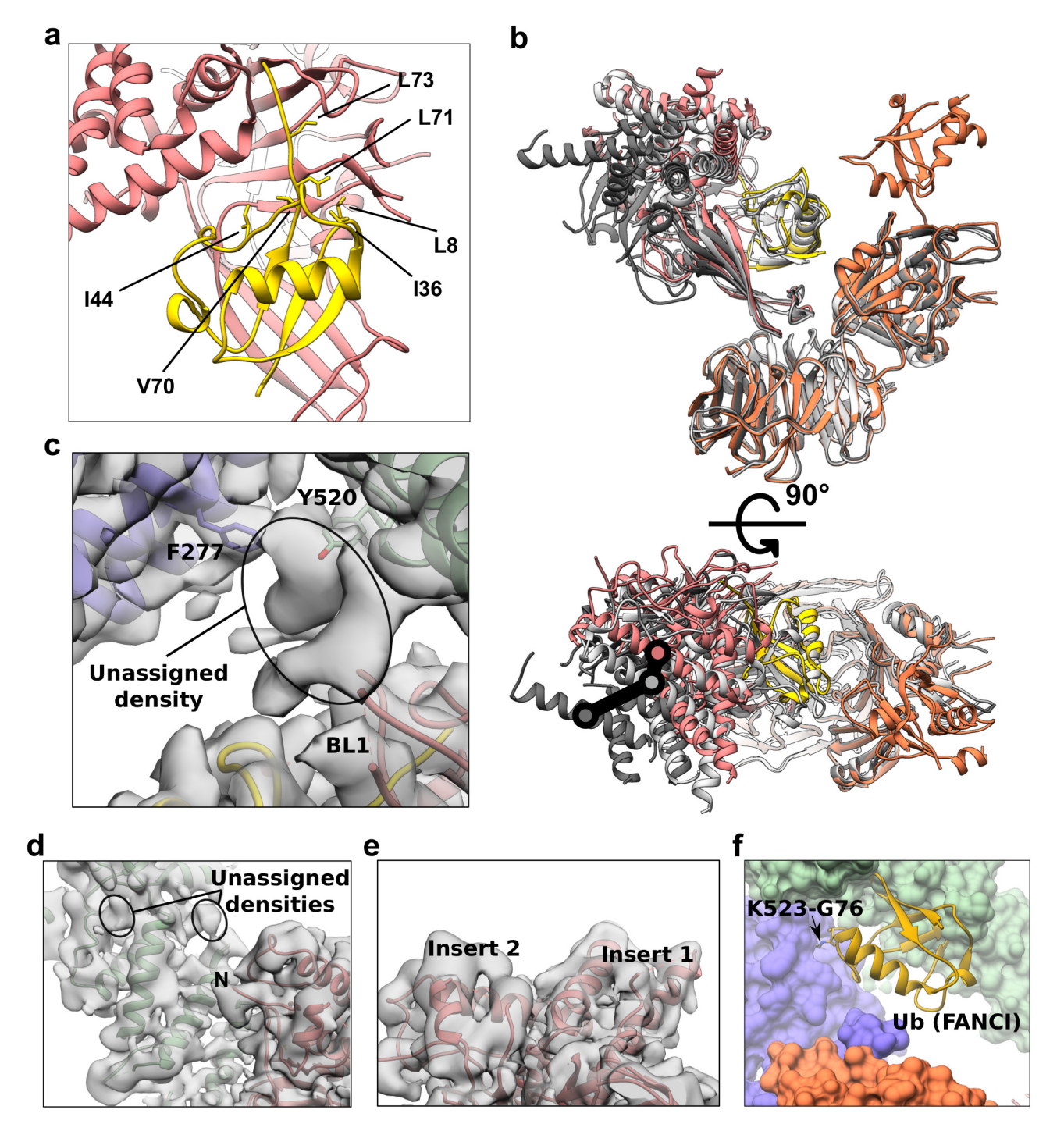
a
L73
L71
L8
I36
I44
V70
b
90°
c
Y520
F277
Unassigned
density
BL1
d
Unassigned
densities
N
e
Insert 2
Insert 1
f
K523-G76
Ub (FANCI)

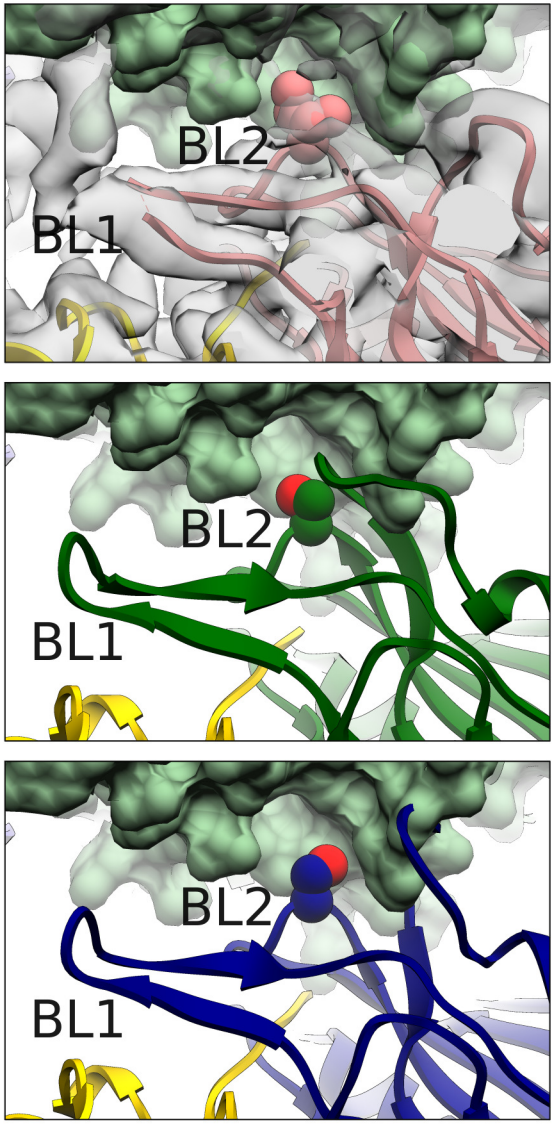
BL2
BL1
BL2
BL1
BL2
BL1